Inclusive Branching Fraction Measurement of $B \to D_s^{\pm} X$ and Search for Direct CP Violation in $B \to D_s^{(*)} D^{(*)}$ at Belle

Master Thesis

Frédéric Dupertuis

Laboratoire de Physique des Hautes Energies
Faculté des Sciences de Base
Ecole Polytechnique Fédérale de Lausanne

Supervisor : **Dr Tagir Aushev**
Professor : **Prof. Olivier Schneider**
External Expert : **Dr Anže Zupanc**

Lausanne 2009-2010

Abstract

The measurement of the inclusive branching fraction $\mathcal{B}(B \to D_s^{\pm} X)$ and the search for direct CP violation (DCPV) in $B \to D_s^{(*)} D^{(*)}$ has been performed with a 710 fb^{-1} data sample recorded by the Belle experiment in Japan.

Preliminary results of inclusive branching fraction $\mathcal{B}(B \to D_s^{\pm} X)$ has been measured with $D_s \to \phi\pi$ decay :

$$\mathcal{B}(B \to D_s^{\pm} X) \quad = \quad (10.06 \pm 0.07\,(\text{stat}) \pm 0.79\,(\mathcal{B}))\,\% \cdot \frac{\mathcal{B}(D_s \to \phi\,\pi)}{(4.39 \pm 0.34)\,\%} \cdot \frac{\mathcal{B}(\phi \to K^+K^-)}{(48.9 \pm 0.5)\,\%}$$

where the first error is statistical and the second one comes from D_s decay branching fraction error and a peaking background estimated to be less than 1 %. Without other systematics evalutation, a 3σ difference to the PDG value has been found.

A compatible with zero DCPV $\mathcal{A}_{\mathcal{CP}}$ in $B \to D_s^{(*)} D^{(*)}$ of $(-0.43 \pm 0.22\ ^{+0.16}_{-0.02})\,\%$ has been found with $D_s \to \phi\pi$ decay.

Contents

Chapter 1

Introduction

During the 2008-2009 academical year, a practical work on Belle detector has been made during the Spring semester for the TPIV project. A full MC study to search for $\Upsilon(5S) \to \Upsilon(4S)\,\pi^0(\to \gamma\gamma)\,\pi^0(\to \gamma\gamma)$ decay using a partial reconstruction technique at Belle has been performed. By computing the recoil mass between $\Upsilon(5S)$ resonance decay and the two reconstructed neutral pions, a peak in this spectrum must emerge at the $\Upsilon(4S)$ resonance mass. A huge combinatorial background has been found. With the selected kinematic cuts, the recoil mass is destroyed, which would make the fit of the spectrum impossible, therefore no strong cuts can be applied. Hence, the conclusion of the invisibility of the $\Upsilon(5S) \to \Upsilon(4S)\,\pi^0(\to \gamma\gamma)\,\pi^0(\to \gamma\gamma)$ at Belle has been claimed due to large combinatorial background.

The reconstruction of the $\Upsilon(5S) \to \Upsilon(4S)\,\pi^+\,\pi^-$ decay has been then tried. A low reconstruction efficiency has been found where only the most energetic pions are reconstructed.

The Master thesis started by continuing the search for $\Upsilon(5S) \to \Upsilon(4S)\,\pi^+\,\pi^-$ decay (see Appendix A). Using a signal MC sample of $\Upsilon(5S) \to \Upsilon(4S)\,\pi^+\,\pi^-$, a huge combinatorial background from the $\Upsilon(4S)$ decay has been found. The search for geometrical cuts has shown that the low momentum tracks have a bad space resolution and no good cuts have been found. Therefore, the conclusion of the invisibility of the $\Upsilon(5S) \to \Upsilon(4S)\,\pi^+\,\pi^-$ decay at Belle has been claimed.

The shift to a new subject has been proceeded to measure the inclusive branching fraction $\mathcal{B}(B \to D_s^{\pm} X)$ and to search for direct CP violation in $B \to D_s^{(*)} D^{(*)}$ which consist the main part of this work.

1.1 Standard Model

The *Standard Model* (SM) is a quantum field theory based on $\mathrm{SU}(3)_C \times \mathrm{SU}(2)_L \times \mathrm{U}(1)_Y$ symmetry group to describe the fundamental interactions between elementary particles. The SM includes the *electroweak model* proposed by Glashow, Weinberg and Salam (GWS) where the $\mathrm{SU}(2)_L \times \mathrm{U}(1)_Y$ group is broken into $U(1)_{EM}$ by the addition of mass terms into the Lagrangian. To get rid of asymptotic behavior of the W-W scattering probability, Higgs proposed its own mechanism to spontaneously break the $\mathrm{SU}(2)_L \times \mathrm{U}(1)_Y \rightarrow U(1)_{EM}$ symmetry group with the help of a scalar field, the *Higgs boson*.

The SM is composed of 6 *quarks* q, 6 *antiquarks* $\bar{q}$, 6 *leptons* l, 6 *antileptons* $\bar{l}$, 14 *gauge bosons* and 1 scalar, the *Higgs boson* h^0. The 6 quarks and leptons are separated in three families :

$$l = \begin{pmatrix} \nu_e \\ e \end{pmatrix}, \quad \begin{pmatrix} \nu_\mu \\ \mu \end{pmatrix}, \quad \begin{pmatrix} \nu_\tau \\ \tau \end{pmatrix} \tag{1.1}$$

$$q = \begin{pmatrix} u \\ d \end{pmatrix}, \quad \begin{pmatrix} c \\ s \end{pmatrix}, \quad \begin{pmatrix} t \\ b \end{pmatrix} \tag{1.2}$$

and the 14 gauge bosons are the 8 *gluons* g to describe the *strong interaction*, the photon γ for the *electromagnetic interaction*, the $W^\pm$ and Z^0 for the *weak interaction* and a hypothetical *graviton* for the *gravitational interaction*.

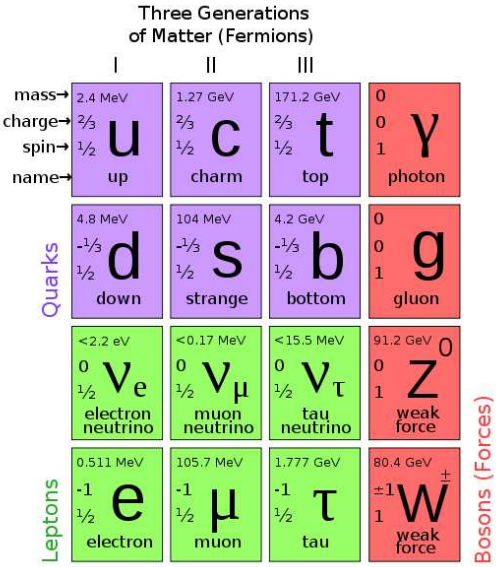

FIGURE 1.1.1: The Standard Model of particle physics

1.2 CP Violation

There are three important discrete symmetries :

- C charge conjugation : replace the particle by its antiparticle
- P parity conjugation : shift all the three space coordinates
- T time reversal : reverse the time backwards, same as reversing the 3-velocity vector

The product of C and P symmetry gives the CP symmetry which links particles and antiparticles world. Therefore looking for *CP violation* (CPV) is to look for different properties, behaviors, asymmetries between the particle and its antiparticle.

Since the discovery of the $K^0 - \bar{K}^0$ mixing and $K_L \to \pi\pi$ CP-violating decay, plenty of other decays and neutral particles mixing have been found related to CP violation. A very good access to CPV comes from B mesons to test the SM and further models of new physics.

Theoretically, the CP violation in SM is only possible with the help of three quark families which quantum states are mixed according to the CKM (Cabibo-Kobayashi-Maskawa) matrix for which Kobayashi and Maskawa received the 2008 Physics Nobel Price.

1.3 Direct CP Violation

The prediction of large CP-violating effects in the B meson system [1] has been confirmed in recent years by the *BABAR* and Belle collaborations, both in the interference of B decays to charmonium final states with and without $B^0 - \bar{B^0}$ mixing [2], and directly in the interference between the decay amplitudes in $B^0 \to K^+\pi^-$ and $B^0 \to \pi^+\pi^-$ [3, 4]. All measurements of CP violation to date are in agreement with indirect predictions from global Standard Model (SM) fits [5] based on measurements of the magnitudes of the elements of the Cabibbo-Kobayashi-Maskawa (CKM) quark-mixing matrix [6] and place important constraints [7] on the flavor structure of SM extensions.

Another interesting decay mode to look for Direct CP Violation (DCPV) is $B \to D_s D$. This decay is a quantum analog to the "golden mode" $B^0 \to J/\psi K_S$ [8] where a $b \to c\bar{c}s$ weak transition occurs. The DCPV in $B \to D_s D$ is due to the interference between the $b \to c$ tree and $b \to s$ penguin decay amplitude and is expected to be small for $B^- \to D_s^- D^0$ (~ 0.2 %) [10] within SM. But some new physics models with new particles participating in penguin loops could give rise to a larger DCPV.

A standard full reconstruction of $D_s D$ was already attempted at Belle, which leads to 2514 ± 64 $\bar{B}^0 \to D_s^- D^+$ events in a sample of $(449 \pm 6) \cdot 10^6$ reconstructed $B\bar{B}$ pairs [11], after extrapolation to the full Belle sample (710 fb^{-1}) this would yield 4322 ± 84 $\bar{B}^0 \to D_s^- D^+$ events and an expected statistical error on the charge asymmetry of 1.4 %.

To improve the statistical error, a partial reconstruction can be used for this mode, where only the D_s is reconstructed, which would give an order smaller error.

The aim of this work is to search for DCPV in $B \to D_s^{(*)} D^{(*)}$ reconstructing only the D_s and to provide a precise measurement of the inclusive branching fraction $\mathcal{B}(B \to D_s^{\pm} X)$ with the full $\Upsilon(4S)$ data sample of Belle.

Chapter 2

Belle Experiment

2.1 KEKB accelerator

KEK laboratory near Tsukuba in Japan uses a 3km long tunnel to run the KEKB e^+e^- accelerator which aim is to provide a beam of electrons e^- and positrons e^+ to the Belle detector located in TSUKUBA area. There is first an electron source that can hit a target to create positrons, that e^-/e^+ are accelerated with a Linac (linear accelerator) which beams are delivered to the HER (High Energy Ring) for electrons and LER (Low Energy Ring) for positrons.

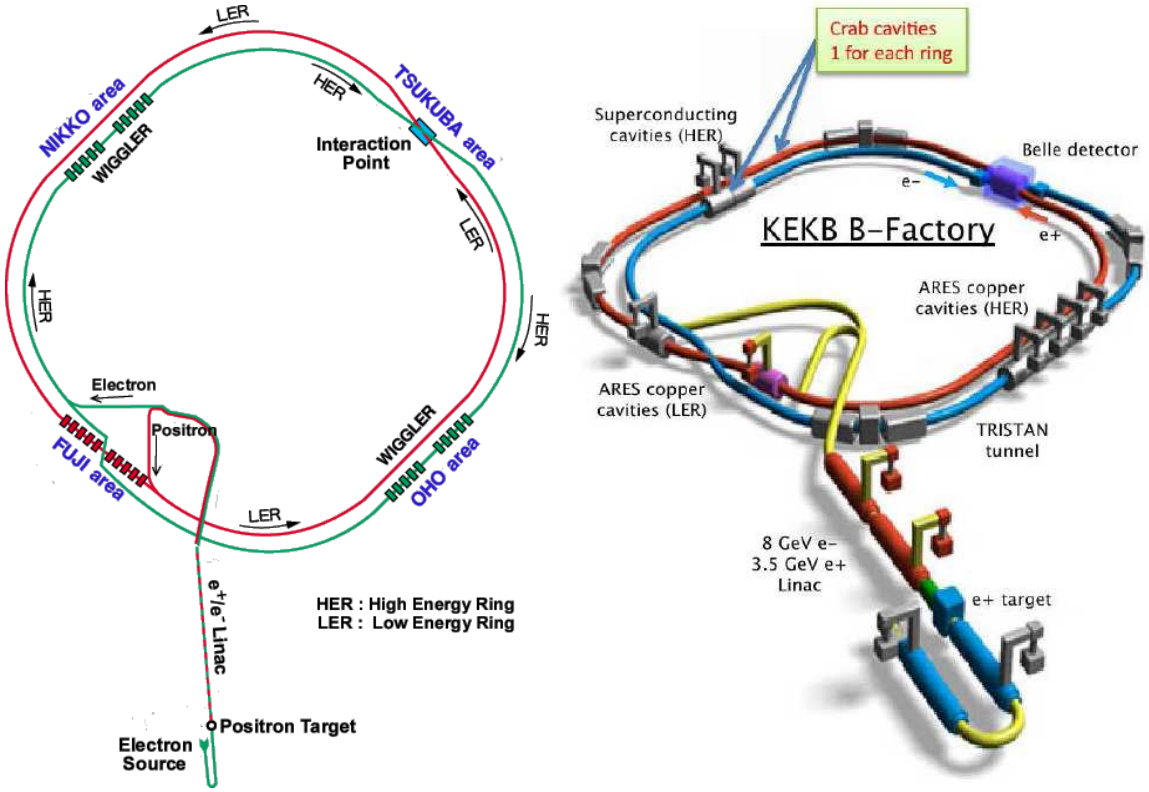

FIGURE 2.1.1: KEKB accelerator

The first goal of the Belle experiment is to study the B mesons that are coming from the $\Upsilon(4S)$ resonance. Due to the small kinetic energy left to the B mesons by the $\Upsilon(4S)$ decay $\Upsilon(4S) \rightarrow B\bar{B}$, the B boost is small in the lab frame. For B oscillation studies, B boost is needed with time dilatation help, therefore an

asymmetry in the e^+e^- energy beam is used as boost for the B mesons. Hence, the KEKB gives an 8 GeV electron beam and 3.5 GeV positron beam to the Belle experiment to create the $\Upsilon(4S)$ resonance at 10.58 GeV. The center of mass energy $\sqrt{s}$ can be calculated and gives approximatively :

$$\sqrt{s} \approx \sqrt{2 \cdot (1 + \cos\theta) \cdot E_{e^+} \cdot E_{e^-}} \tag{2.1}$$

where θ is the crossing angle of 22 mrad between the two beams and E_{e^-}, E_{e^+} the electron and positron energy respectively. With 8 GeV and 3.5 GeV for electron and positron beam energy respectively, the center of mass energy gives the $\Upsilon(4S)$ mass of 10.58 GeV/c^2.

The KEKB accelerator has worked and still working at other $b\bar{b}$ resonance such as $\Upsilon(1S)$, $\Upsilon(2S)$, $\Upsilon(3S)$ and $\Upsilon(5S)$. The $\Upsilon(5S)$ mass is above $B_s\bar{B}_s$ threshold which gives access to B_s mesons with B-factories such as CLEO, BaBar and Belle experiments for example.

Using a high intensity beam (5000 bunches per beam distributed along 3km tunnel) and with the help of "crab cavities", the Belle detector carries the luminosity world record of $2.11 \cdot 10^{34}$ cm$^{-2} \cdot$ s^{-1} and has accumulated a total integrated luminosity world record of 1000 fb^{-1}.

2.2 Belle detector

Belle is an asymmetric full solid angle detector specially designed for B physics. Figure 2.2.1 shows a XZ view of the detector.

The Belle detector is made of the following subdetectors from the inner to the outer part :

- SVD2 (Silicon Vertex Detector) is used for vertexing and tracking. The vertex detector is made of four silicon layers which z resolution reaches 100 μm.
- CDC (Central Drift Chamber) is used for tracking with the magnetic field of 1.5 T provided by a superconducting solenoid and particle identification.
- ACC (Aerogel Cherkenov Counter) is used for particle identification to separate kaons from pions.
- TOP (Time Of Flight) is used for particle identification.
- CsI or ECL (Electromagnetic CaLorimeter) and EFC (Electromagnetic Forward Calorimeter) is used for measuring photons and electrons/positrons energy.
- KLM (K Long/Muon) is used to detect muons and K_L mesons.

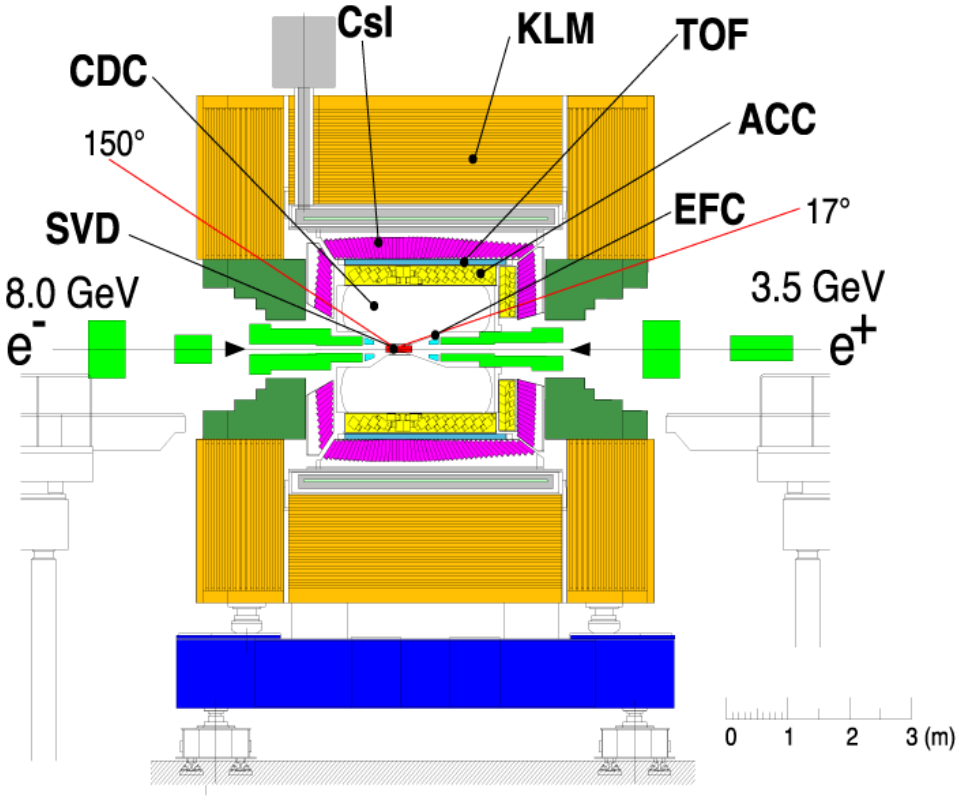

FIGURE 2.2.1: XZ view of Belle detector

2.3 Particle Identification

First, the CDC can measure the dE/dx (deposed energy within a step length dx) for charged particle which can be compared to deposit energy models knowing the measured momentum of the track by the CDC.

Second, the ACC is based on Cherenkov effect where a particle flying faster than the speed of light in the silica aerogel medium, will emit Cherenkov light. Having or not light can separate kaons and pions for momentum range of $1.2 \leq p \leq 3.5$ GeV/c. In this region, pions emit light where kaons not.

Last, the TOF is measuring the time between the e^+e^- collision provided by the KEKB clock and the hit time in TOF modules. With this method, the mass can be measured :

$$m\,\frac{v^2}{R} = q\,v\,B \Longrightarrow m\,v = q\,v\,B = p = m\,\frac{\Delta s}{\Delta t} \Longrightarrow m = p\,\frac{\Delta t}{\Delta s} \tag{2.2}$$

where p is the measured momentum by the CDC, Δs the track length between the IP and hit point, Δt the time between interaction and hit in TOF modules.

For each of these three subdetectors and particle assumption, they provide a likelihood function $\mathcal{L}$ for particle selection.

2.4 Tracking

A particle, within a magnetic field, traversing matter will follow an helix in magnetic normal plan. The infinitesimal curvature radius of the helix gives the particle momentum for a given magnetic field norm and direction, and the speed at which the radius decreases is given by the energy deposit dE/dx by the particle. Therefore, assuming an energy deposit dE/dx of a particle and with the magnetic field map, the momentum can be computed with helix fit of CDC hits.

2.5 Software

2.5.1 Belle Software

The Belle framework called *BASF* (Belle AnalysiS Framework) is able to provide :

1. A unified and standalone access to the data with a memory management system called *Panther*.
2. Event-by-event parallel processing.
3. Fortran, C and C++ modules interpretor.
4. Modules processing on data.
5. Data outputs saving.

For the MC production, two softwares are used :

1. *EvtGen* : Generate the required events coming from the e^+e^- interaction such as $e^+e^- \rightarrow \Upsilon(4S) \rightarrow B^0(\rightarrow D_s^+ D^-)\,\bar{B}^0$ or $e^+e^- \rightarrow \Upsilon(5S) \rightarrow \Upsilon(4S)\ \pi^+\ \pi^-$.
2. *GEANT* : Create the particle interactions with matter, tracking in magnetic field, detector effects, event visualization and data storage in *MDST* format.

The event reconstruction is made using a module with a specific structure and saves the results in *HBOOK* format.

2.5.2 Analysis Software

The analysis is made using *ROOT* and *RooFit* software. The HBOOK information storage is made for PAW software, to use these HBOOK with ROOT, the *h2root* application is used for conversion. For each analysis part, a dedicated ROOT/RooFit script is written.

Chapter 3

Inclusive Branching Fraction measurement

The decay of B mesons into final states involving a $D_s^{(*)+}$ provides an opportunity to study the production mechanisms for $c\bar{s}$ quark pairs. Although several diagrams can lead to $D_s^{(*)+}$ production in B decays, the dominant source [13] is expected to be external $W^+ \to c\bar{s}$ emission. A precise knowledge of this production rate remains interesting in light of continuing theoretical difficulties [14] in accounting for the measurements of both the semileptonic branching fraction and the inclusive charm production rate in B decays. Indeed, it has been noted that an enhanced B decay rate to charm would help explain the small observed semileptonic rate [15].

It is possible to produce $D_s^{(*)+}$ mesons in $q\bar{q}$ events from continuum e^+e^- annihilation. The process of fragmentation (*i.e.*, formation of hadrons) is nonperturbative and can only be modeled phenomenologically. The ratio of vector to pseudoscalar production rates is of particular interest for testing such models. The D_s^+ system is well suited to measure this quantity because the $c\bar{s}$ states with $L = 1$ have not been observed to decay to either D_s^+ or D_s^{*+} mesons.

3.1 Inclusive generated D_s momentum spectrum

Figure 3.1.1 shows the generated inclusive D_s momentum spectrum (EvtGen) at the generator level and center of mass given by the $\Upsilon(4S)$ resonance mean energy.

The spectrum presents two distinct components : one with D_s mesons from B decays and one with D_s mesons produced in the continuum. In the left part, there are mainly D_s coming from B *decay* and a small fraction from udsc continuum, and in the right part, it's *pure continuum*. This separation comes from different kinematics between D_s from B decay and continuum.

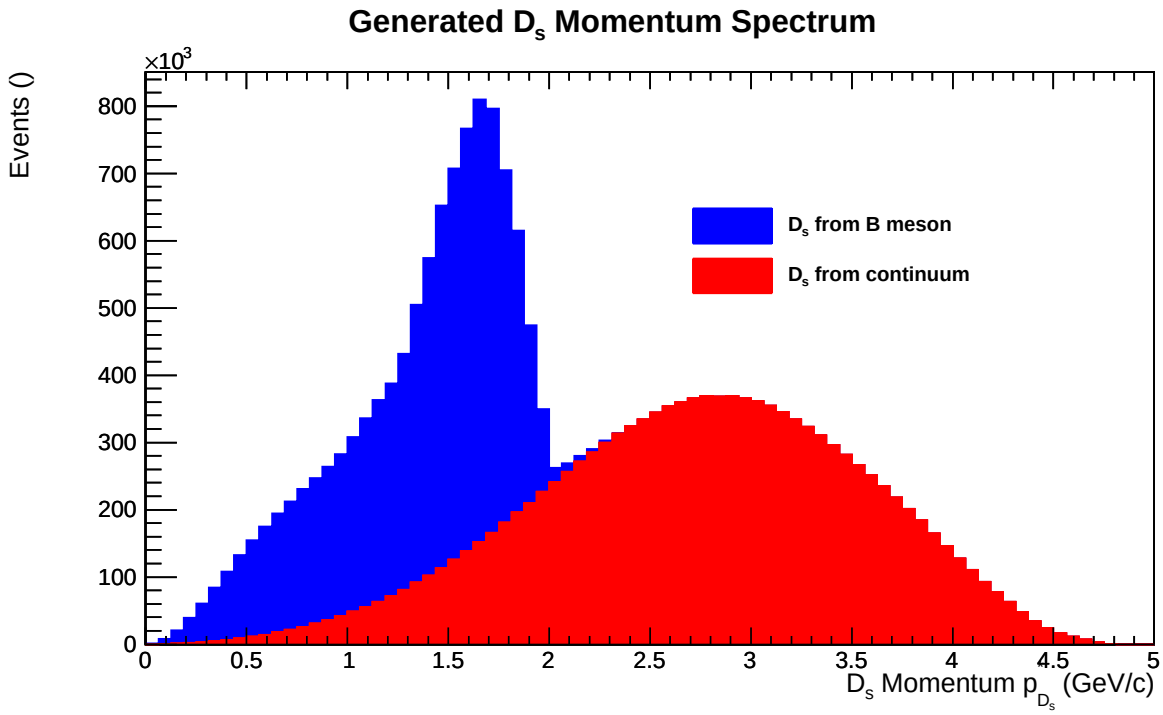

FIGURE 3.1.1: EvtGen D_s^+ Momentum Spectrum

3.1.1 D_s kinematics

The maximum D_s momentum available in continuum comes from $e^+e^- \to D_sD_s$.

$$p^*_{e^+e^-} = \begin{pmatrix} \sqrt{s} \\ \vec{0} \end{pmatrix} = p^*_{D_s^+} + p^*_{D_s^-} = \begin{pmatrix} \sqrt{m^2_{D_s} + p^{*2}_{D_s^+}} \\ \vec{p^*_+} \end{pmatrix} + \begin{pmatrix} \sqrt{m^2_{D_s} + p^{*2}_{D_s^-}} \\ \vec{p^*_-} \end{pmatrix} \tag{3.1}$$

which gives $\left|\vec{p^*_+}\right| = \left|\vec{p^*_-}\right| = p^*_{D_s} = \sqrt{\left(\frac{\sqrt{s}}{2}\right)^2 - m^2_{D_s}} \approx 4.91$ GeV/c with available energy in e^+e^- frame of $\sqrt{s} = 10.58$ GeV at the $\Upsilon(4S)$ resonance. And the maximum D_s momentum available in B decay comes from $B \to D_s\pi$ with lightest meson made of u/d quark, the computation gives $p^{**}_{D_s} \approx 2.27$ GeV/c in B frame. The D_s momentum from $B \to D_sD$ is $p^{**}_{D_s} \approx 1.81$ GeV/c.

3.1.2 $B \to D_s^{(*)}D^{(*)}$ decay

There is a clear region of B decay which comes from $B \to D_s^{(*)}D^{(*)}$ (see Figure 3.1.2). The structure of this region comes from $\Upsilon(4S) \to B\bar{B}$ decay properties. The momentum left to B mesons in $\Upsilon(4S)$ rest frame is 328 MeV/c. Compared to the D_s momentum of 1.81 GeV/c coming from B decay in B frame, the D_s momentum is like a monochromatic peak smeared by the B momentum, which direction is isotropic because coming from the spinless $\Upsilon(4S)$ resonance.

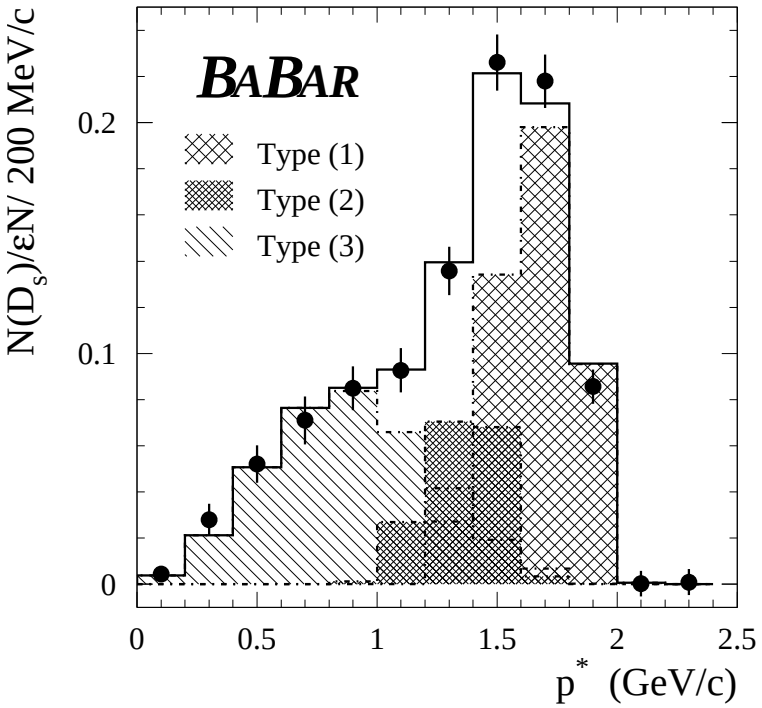

FIGURE 3.1.2: D_s Momentum Spectrum with three decay types where *Type 1* is $B \to D_s^{(*)} D^{(*)}$, *Type 2* is $B \to D_s^{(*)} D^{(**)}$ and *Type 3* is $B \to D_s^{(*)} D^{(*)} \pi/\rho/\omega$ [12]

3.2 Inclusive Branching Fraction of $B \to D_s^{\pm} X$ Measurement Technique

3.2.1 Generic MC, $\Upsilon(4S)$ and continuum data samples

The *generic MC* is a MC sample aiming at the most general description of e^+e^- interactions, including the production and decay of the $\Upsilon(4S)$, using the knowledge available of branching fractions, luminosity, detector parameters, experimental conditions, ...

There are four types of generic MC at the $\Upsilon(4S)$ resonance :

- *charged* for $e^+e^- \to \Upsilon(4S) \to B^+B^-$ decay
- *mixed* for $e^+e^- \to \Upsilon(4S) \to B^0\bar{B}^0$ decay
- *uds* for $e^+e^- \to q\bar{q}$ with $q = u, d, s$ hadronization
- *charm* for $e^+e^- \to c\bar{c}$ hadronization

Then, the sum of charged and mixed is the *B decays* and the sum of uds and charm is the *continuum*. There are ten streams of charged/mixed and six streams of uds/charm available.

Two types of data samples are available, the *on_resonance* sample where the accelerator works at the peak of the $\Upsilon(4S)$ resonance ($\sqrt{s} = 10.58$ GeV) and the *continuum* sample selected 60 MeV under the $\Upsilon(4S)$ mass peak and $B\bar{B}$ threshold.

3.2.2 D_s yield scaling and B decay extraction

Using the generic MC, the *MC reconstruction efficiency* $\epsilon^{\pm}_{MC}$ can be obtained. In the assumption that the MC simulation is in a good agreement with reality, the real reconstruction efficiency $\epsilon^{\pm}$ can be considered as equal to the MC reconstruction efficiency $\epsilon^{\pm}_{MC}$. Then, the reconstructed momentum spectrum can be corrected and scaled bin by bin using the momentum dependent reconstruction efficiency as $N_{exp}(p^*_{D_s}) = N_{reco}(p^*_{D_s})/\epsilon_{MC}(p^*_{D_s})$ to obtain an expected real momentum spectrum.

The B decay events yield can be extracted from the $\Upsilon(4S)$ and continuum data sample. The basic idea is to subtract the $\Upsilon(4S)$ and continuum sample momentum spectrum after yield scaling with their corresponding reconstruction efficiencies. But the two samples do not have the same *integrated luminosity* $\mathcal{L}$ and running energy E. The integrated luminosity is the quantity which multiplied by the cross section σ of a process gives the expected event yield of the given process. The hadronic cross section σ is energy dependent like $\sigma \propto E^{-2}$. In addition, the momentum available at the continuum and on resonance is not the same, then the momentum has to be scaled to the $\Upsilon(4S)$ case, hence a momentum-less quantity $x^*_p = \frac{p^*_{D_s}}{p^*_{D_s,max}}$ is introduced with $p^*_{D_s,max}$ the maximum D_s possible momentum which is from $e^+e^- \to D_sD_s$ ($p^*_{D_s,max}$ = 4.909 GeV/c on resonance and $p^*_{D_s,max}$ = 4.877 GeV/c on continuum). Then, the continuum sample momentum spectrum can be scaled to $\Upsilon(4S)$ sample one for subtraction and the total expected B events yield N^B_{exp} (sum of each momentum bins) is given by :

$$N^B_{exp} = \sum_{x^*_p} \left(\frac{N^{\Upsilon(4S)}_{reco}(x^*_p)}{\epsilon^{\Upsilon(4S)}(x^*_p)} - \frac{N^{cont}_{reco}(x^*_p)}{\epsilon^{cont}(x^*_p)} \cdot \frac{\mathcal{L}_{\Upsilon(4S)}}{\mathcal{L}_{cont}} \cdot \frac{E^2_{cont}}{E^2_{\Upsilon(4S)}} \right) \tag{3.2}$$

with $N^{\Upsilon(4S)}_{reco}$ and N^{cont}_{reco} the reconstructed yield, $\mathcal{L}_{\Upsilon(4S)}$ and $\mathcal{L}_{cont}$ the integrated luminosity, E_{cont} and $E_{\Upsilon(4S)}$ the energy available in e^+e^- frame, $\epsilon^{\Upsilon(4S)}$ and ϵ^{cont} the reconstruction efficiency in $\Upsilon(4S)$ and continuum conditions/sample respectively. For better precision, the scale factor $\Lambda = \frac{\mathcal{L}_{\Upsilon(4S)}}{\mathcal{L}_{cont}} \cdot \frac{E^2_{cont}}{E^2_{\Upsilon(4S)}}$ can be obtained from a constant fit of the $\Upsilon(4S)$/continuum spectrum ratio. The two scale factors will be measured/calculated.

3.2.3 Inclusive Branching Fraction $\mathcal{B}(B \to D^{\pm}_s X)$ computation

Experimentally, only few clean D_s channels are reconstructed, then the generated B events yield $\tilde{N}^B_{i,gen}$ of each channel is a subset of the total yield N^B_{gen} : $\tilde{N}^B_{i,gen} = \mathcal{B}(D_s \to i) \cdot N^B_{gen}$ where $\mathcal{B}(D_s \to i)$ is the branching fraction of chosen channel i. The reconstructed D_s yield $\tilde{N}^B_{i,reco}$ is given, with the reconstruction efficiency $\epsilon_{i,MC}$, by :

$$\tilde{N}^B_{i,reco} = \tilde{N}^B_{i,gen} \cdot \epsilon_{i,MC} \tag{3.3}$$

Taking into account that two B mesons come from the $\Upsilon(4S)$ decay which yield is given by $N_{B\bar{B}}$, the fraction of B admixture decaying to $D^{\pm}_s$, ie $\mathcal{B}(B \to D^{\pm}_s X)$, can be extracted from :

$$\tilde{N}^B_{i,gen} = N_{B\bar{B}} \cdot 2 \cdot \mathcal{B}(B \to D^{\pm}_s X) \cdot \mathcal{B}(D_s \to i) \tag{3.4}$$

Finally, the measured inclusive branching fraction $\mathcal{B}_i(B \to D^{\pm}_s X)$ is given by :

$$\mathcal{B}_i(B \to D^{\pm}_s X) = \frac{1}{2 \cdot N_{B\bar{B}}} \cdot \frac{\tilde{N}^B_{i,reco}}{\mathcal{B}(D_s \to i) \cdot \epsilon_{i,MC}} \tag{3.5}$$

where the index i stands for the chosen channel.

3.3 D_s Reconstruction Method

In order to reach a high purity sample and good reconstruction efficiency, the D_s meson is reconstructed using three clean decay modes : $D_s^- \to \phi(\to K^+K^-)\pi^-$, $D_s^- \to K_S^0(\to \pi^+\pi^-)K^-$ and $D_s^- \to K^{*0}(\to K^+\pi^-)K^-$. The known branching fraction of these decays are given in Table 3.3.1.

	$\mathcal{B}(\%)$
$D_s^- \to \phi(\to K^+K^-)\pi^-$	(2.15 ± 0.17)
$D_s^- \to K_S^0(\to \pi^+\pi^-)K^-$	(1.03 ± 0.06)
$D_s^- \to K^{*0}(\to K^+\pi^-)K^-$	(2.6 ± 0.4)

TABLE 3.3.1: Branching fraction of reconstructed decays [9]

Hence the total reconstructed branching fraction is $(5.78 \pm 0.44)\,\%$.

3.3.1 Reconstruction in Belle Framework

All charged tracks are listed in the `MDST_CHARGED` table. Lists of kaons and pions, with their 4-momenta, are first filled with each track from the table assuming the dE/dx of the given particle and the magnetic field map for the helix parametrization. Then pions and kaons are separated using the likelihood given by the CCD, TOF and ACC subdetectors and cutting on the following likelihood ratio :

$$\mathcal{R}_{K/\pi} = \frac{\mathcal{L}(K)}{\mathcal{L}(K) + \mathcal{L}(\pi)} \tag{3.6}$$

The probability to be a kaon increases when this ratio goes to 0 and to 1 for the pions. In the Belle framework, the *kaon ID* is defined to be $\mathcal{R}_{K/\pi}$ and the *pion ID* to be $1 - \mathcal{R}_{K/\pi}$, which is compatible with the probability definition. These particle ID's are first cuts that can be performed to increase the sample purity. In reality, only the kaon ID will be used as cut. The multiplicity of pions in an event is much higher than the kaon one, which means that cutting strongly on the pion ID will throw out mostly pions for small number of kaons, which is not efficient. Only a soft cut of 0.9 on $\mathcal{R}_{K/\pi}$ is applied to get rid of large kaon yield between $\mathcal{R}_{K/\pi} \in [0.9, 1]$. A tight cut on $\mathcal{R}_{K/\pi}$ of 0.1 is used as starting point for cut selection to suppress most of the pions that are between $\mathcal{R}_{K/\pi} \in [0, 0.1]$.

In addition, pions and kaons are required to have an impact parameter in the radial direction (δr) less than 2 cm and a beam axis distance (δz) less than 4 cm, because particles must come from the neighborhood of the Interaction Point (IP).

- For the K_S^0 reconstruction via $K_S^0 \to \pi^+\pi^-$ ($\mathcal{B}(K_S^0 \to \pi^+\pi^-) = (69.20 \pm 0.05)\%$ [9]), a dedicated class `Find_Ks` is used to select them and its `good_Ks_loose` method [16]. The class takes two oppositely charged tracks from `MDST_CHARGED` without particle ID. Four variables are used for selection : the distance along the beam dz from which tracks start, the smallest impact parameter among the two tracks dr, the $r_{K_S^0}$ distance in the $r - \phi$ plane between the K_S^0 vertex and the IP, the angle between the K_S^0 momentum and the direction joining the IP to the K_S^0 vertex. The K_S^0 is a long-lived particle, so it can decay anywhere from IP to CDC, which gives 3 different cases : zero, one or two daughters have matching hits in SVD (Table 3.3.2).

Case	dr (cm)	dz (cm)	$r_{K_S^0}$	$\Delta\phi$
2 daughters have matching hits in SVD	> 0.03	< 0.35	< 2	> 0.08
Only 1 daughter has matching hits in SVD	> 0.10	< 0.40	< 40	< 9.0
No daughter has matching hits in SVD	> 0.10	< 0.05	< 6.5	> 1.5

TABLE 3.3.2: Geometrical requirements of `good_Ks_loose` for K_S^0 reconstruction [16]

- For $\phi \to K^+K^-$ ($\mathcal{B}(\phi \to K^+K^-) = (48.9 \pm 0.5)\,\%$ [9]), two opposite charged kaons are combined and the reconstructed mass is required to be in a large window of $\pm$ 60 MeV. The reconstructed ϕ mass is saved for further cut selection.

- For $K^{*0} \to K^+\pi^-$ ($\mathcal{B}(K^{*0} \to K^+\pi^-) = (\frac{2}{3} \times (99.77 \pm 0.02)\,\%$ [9]), a positively charged kaon is combined with a negatively charged pion. Then reconstructed mass is required to be within a $\pm$ 100 MeV window. This window is rather tight because of the huge combinatorial background before cut selection.

- Finally, the D_s^- is reconstructed according to the three chosen decays and the invariant mass is required to be in a window of $\pm$ 80 MeV. This range is large enough to allow large sidebands for background evaluation and small enough to avoid keeping a large amount of background.

The $D_s \to \phi(\to KK)\pi$ and $D_s \to K^{*0}(\to K\pi)K$ are scalar to vector scalar transition with vector to two scalars decay lead to a $\cos^2(\theta_h)$ distribution of the helicity angle θ_h. This *helicity angle* or *polar angle* is defined as the angle between the incoming momentum of the mother and one of the vector's daughter in the vector frame. Moreover, the background is expected to be more or less flat, which gives a cut for signal selection where the center part of the distribution is cut.

And finally, a vertex fit is computed to get rid of combinatorial background. In reality, the D_s^- is reconstructed with the three particles, for example $K^+K^-\pi^-$ for $\phi\pi^-$ and then ask for ϕ mass window. The two daughters of the ϕ are strongly boosted in the e^+e^- rest frame due to the small ϕ mass compared to D_s^- one, which leads to a very small crossing angle of the two tracks. If a vertex fit would be computed for the ϕ particle, the vertex will be not effective. In this way and because the ϕ meson does not fly due to its strong decay, the vertex fit is performed on the combined vertex of the three particles. The result of this vertex fit gives a χ^2 that can be used for combinatorial background suppression.

3.3.2 Reconstruction with Data and Generic MC

The advantage of the generic MC is the availability of the generation information (*GenHep*), or the so-called "*MC truth*", gives some extra informations such as the mother ID of a given particle. For example, asking the mother of the two kaons to be a ϕ and the grandmother of these kaons and the mother of the pion to be a D_s, gives the true reconstructed inclusive D_s yield, mass, momentum spectrum ... decaying to $\phi\pi$. Table 3.3.3 summarizes the variables saved in HBOOK structures for data and generic MC cases.

Ntuple	Internal Name	Description
h1	momds	D_s momentum in the e^+e^- rest frame
	massds	D_s mass
	massphi	ϕ mass
	masskst	K^{*0} mass
	massks	K^0_S mass
	polarphi	Helicity angle θ_h of ϕ
	polarkst	Helicity angle θ_h of K^{*0}
	chgds	D_s charge
	kid1	Kaon ID of 1^{st} kaon
	kid2	Kaon ID of 2^{nd} kaon
	pid1	Pion ID of pion
	vchids	Vertex fit χ^2
	chds	D_s channel
	mid1	*GenHep* : Mother ID of 1^{st} particle
	mid2	*GenHep* : Mother ID of 2^{nd} particle
	mid3	*GenHep* : Mother ID of 3^{rd} particle
	...	...
	mmmmid3	*GenHep* : GrandgrandgrandMother ID of 3^{rd} particle
h2	momds	*GenHep* : D_s momentum in the e^+e^- rest frame
	chgds	*GenHep* : D_s charge
	chds	*GenHep* : D_s channel

TABLE 3.3.3: The HBOOK structure and main recorded variables. Black variables are filled for both data and generic MC while in red are filled only for generic MC

3.3.3 Reconstruction Script

For handling simplicity, the three decays are reconstructed together. Two channels are defined (`chds`), the first one is $D_s^- \to K^+K^-\pi^-$ and the second one is $D_s^- \to K^0_S K^-$. In the first case, the ϕ mass is computed for the two first particles and the K^{*0} mass using the two last particles with range requirements described in previous section, similarly for the helicity angle. For the second channel, particle IDs, `kid2`, `pid1` and mother IDs *mid3*,...,*mmmmid3* are set to 0.

3.3.4 D_s yield extraction

In order to obtain the significance for each cut, the number of signal and background must be extracted. Two methods are chosen, the first is fitting the overall shape of the D_s mass and extract the yield of each contributions. The second one is based on a sideband method, which consists of fitting the sidebands with a given function and estimate the background yield in the signal region. By subtraction of this estimation from the total number of events in the signal region, the expected number of D_s events can be computed.

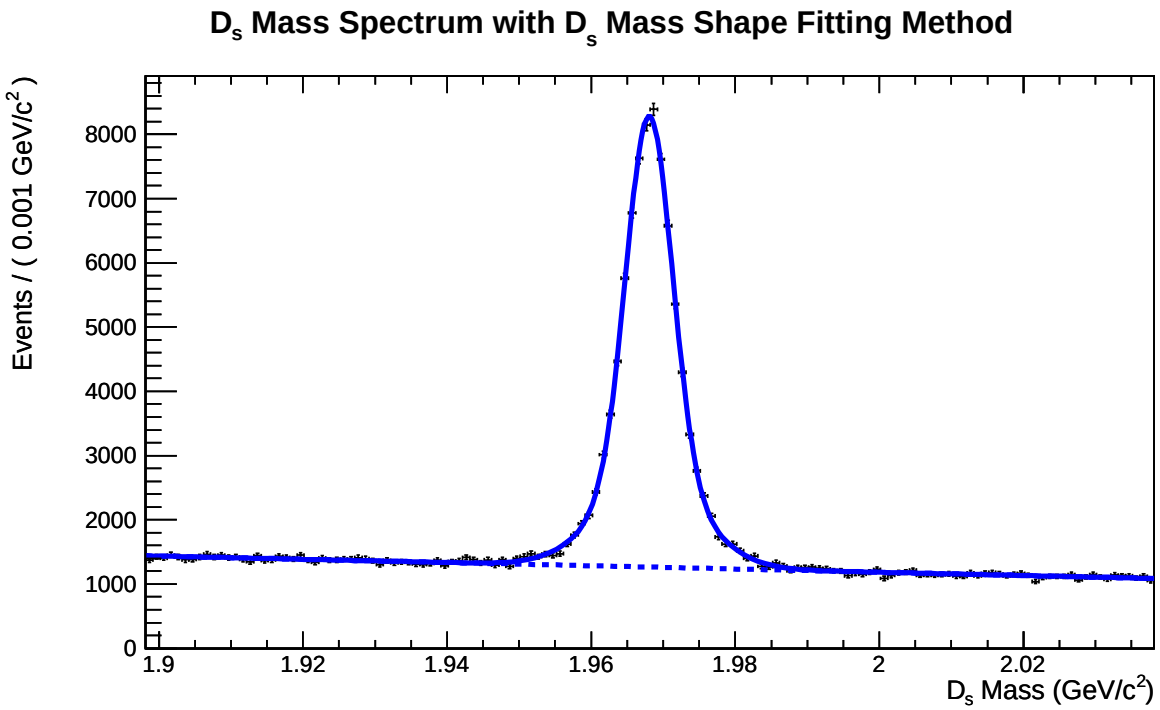

FIGURE 3.3.1: Example of D_s Mass Spectrum with Fitting Method

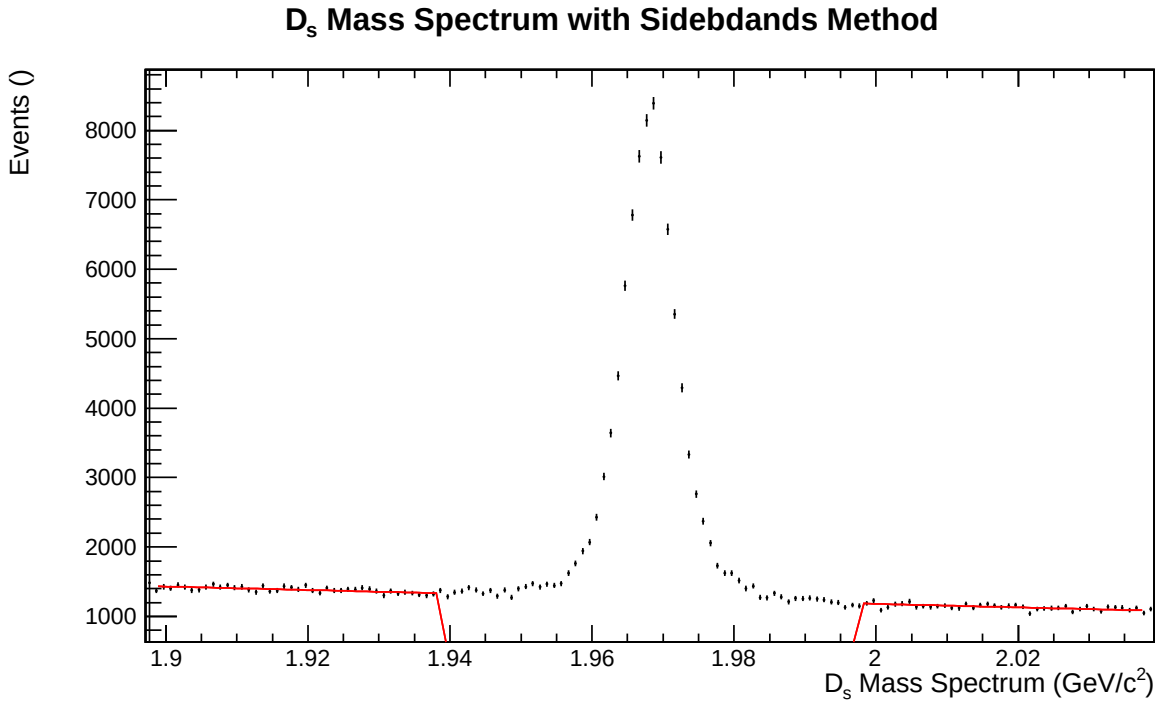

FIGURE 3.3.2: Example of D_s Mass Spectrum with Sidebands Method

D_s mass fitting method

The D_s particle is the lightest $c\bar{s}$ meson : it decays weakly, hence its own width is negligible and the spread of the D_s mass spectrum is purely due to resolution. The signal is parametrized using a double Gaussian with a common mean. For the background, a slope function is used. Then, the D_s mass spectrum function f is given by :

$$\begin{aligned}(m_{D_s}; f_g, \mu, \sigma_1, \sigma_2, c) &= N_{sig} \cdot \left\{ f_g \cdot \frac{G(m_{D_s}; \mu, \sigma_1)}{\int_\Omega [G(m_{D_s}; \mu, \sigma_1)]\, dm_{D_s}} + (1 - f_g) \cdot \frac{G(m_{D_s}; \mu, \sigma_2)}{\int_\Omega [G(m_{D_s}; \mu, \sigma_2)]\, dm_{D_s}} \right\} \\ &+ N_{bkg} \cdot \frac{1 + c \cdot m_{D_s}}{\int_\Omega (1 + c \cdot m_{D_s})\, dm_{D_s}} \end{aligned} \tag{3.7}$$

where $G(m_{D_s}; \mu, \sigma)$ is the Gaussian distribution function of D_s mass m_{D_s} with mean value μ and standard deviation σ, f_g the fraction of the first Gaussian, c the slope parameter, N_{sig} the signal yield, N_{bkg} the background yield and Ω the mass spectrum range.

Sidebands subtraction method

The sidebands method is based on background under signal evaluation with the help of sidebands made of pure background. This background in signal region $N_{bkg,\Omega_{sig}}$ can be computed, in a linear background assumption, as :

$$N_{bkg,\Omega_{sig}} = \frac{N_{low} + N_{high}}{2} \cdot \frac{|\Omega_{sig}|}{|\Omega_{low,high}|} \tag{3.8}$$

where N_{low}, N_{high} are the events yield in lower and higher sideband respectively, $|\Omega_{sig}|$ the signal window width and $|\Omega_{low,high}|$ the common sideband window width.

To improve the event yield estimation in sidebands, a slope function can be used to fit them. This function normalization can be set in such a way to include the background under signal yield in the fit as :

$$f(m_{D_s}; \mu, c, \Omega_{sig}, \Omega_{low,high}) = N_{bkg,\Omega_{sig}} \cdot \frac{|\Omega_{low,high}|}{|\Omega_{sig}|} \frac{2 \cdot [1 + c \cdot (m_{D_s} - \mu)]}{\int_{\Omega_{low} \cup \Omega_{high}} [1 + c \cdot (m_{D_s} - \mu)]\, dm_{D_s}} \tag{3.9}$$

where μ is the D_s mass from PDG [9] and c the slope parameter. Then, the signal yield can be obtained by subtraction as $N_{sig} = N_{\Omega_{sig}} - N_{bkg,\Omega_{sig}}$, where $N_{\Omega_{sig}}$ is the total number of events in the signal window.

3.3.5 Cut Selection

The goal of the cut selection is to maximize the signal significance $\frac{S}{\sqrt{S+B}}$, where S is the signal yield and B the background yield, in the cut variables multidimensional space. For this analysis, the cut selection can be done on data instead of MC because based on optimization of signal yield with the help of D_s mass spectrum, where the interesting quantity for this analysis is the D_s momentum spectrum shape, therefore no bias can be created by this optimization.

The Table 3.3.4 summarize the cuts that are used for purity enhancement.

Cut Internal Name	Cut Description
`kid1`, `kid2`	Kaon ID $\mathcal{R}_{K/\pi}$
`massphi`, `massks` or `masskst`	ϕ, K^0_S or K^{*0} mass
`polarphi` or `polarkst`	Helicity angle θ_h of ϕ and K^{*0}
`vchids`	D_s^- Vertex fit χ^2

TABLE 3.3.4: Available Cuts for Selection

In order to find the optimum, the variables are assumed to be independent, hence the selection can be done by setting the cuts one after the other, rather than scanning a multidimensional space. The first cut is made on the Kaon ID to purify the K sample before further combinatorial background suppression. Then, the three other selection cuts are applied in the order given by Table 3.3.4.

The cut on Kaon ID is performed using a $\pm 1\,\sigma$ window around the $\phi/K^{*0}/K^0_S$ mass to really find the best cut for the given decay and not for inclusive kaons. The σ is obtained by single Gaussian χ^2 fit to the mass. The result are given in Table 3.3.5.

	ϕ	K^{*0}	K^0_S
σ (MeV/c^2)	8	32	3.5

TABLE 3.3.5: Single Gaussian width results of a χ^2 fit to the $\phi/K^{*0}/K^0_S$ mass

The signal significance is plotted in Figure 3.3.3, 3.3.4 and 3.3.5 as a function of the cut values. The optimum results are summarized in Table 3.3.6.

Decay	Significance $\frac{S}{\sqrt{S+B}}$	Kaon ID	$\phi/K^{*0}/K^0_S$ Mass	$\lvert\cos(\theta_h)\rvert$	Vertex Fit χ^2
$\phi\pi$	223	> 0.6	$\pm$ 10 MeV/c^2	> 0.4	< 16
$K^{*0}K$	145	> 0.6	$\pm$ 40 MeV/c^2	> 0.5	< 9
K^0_SK	101	> 0.6	$\pm$ 8 MeV/c^2	-	< 9

TABLE 3.3.6: Cut Selection Results

Some of these results have been obtained using a single gaussian instead of a double gaussian, because for kaon ID and K^{*0}/K^0_S mass selection the purity of $K^{*0}K$ and K^0_SK decays was too low to be enough sensitive to a double Gaussian fit and gave unstable results. The cut on kaon ID of 0.6 has been selected because its induced systematic is well known, even if it is not the best cut. Using the cuts of Table 3.3.6, sub-ROOT files for each decays are created saving only the needed parameters summarized in Table 3.3.7 for the analysis.

Ntuple	Internal Name	Description
h1	`momds`	D_s momentum in the e^+e^- rest frame
	`massds`	D_s mass
	`chgds`	D_s charge
	`mid1`	*GenHep* : Mother ID of 1^{st} particle
	`mid2`	*GenHep* : Mother ID of 2^{nd} particle
	`mid3`	*GenHep* : Mother ID of 3^{rd} particle
	...	...
	`mmmmid3`	*GenHep* : GrandgrandgrandMother ID of 3^{rd} particle
h2	`momds`	*GenHep* : D_s momentum in the e^+e^- rest frame
	`chgds`	*GenHep* : D_s charge

TABLE 3.3.7: The final structure of ROOT files for analysis with recorded variables (in black for both data and generic MC and in red only for generic MC)

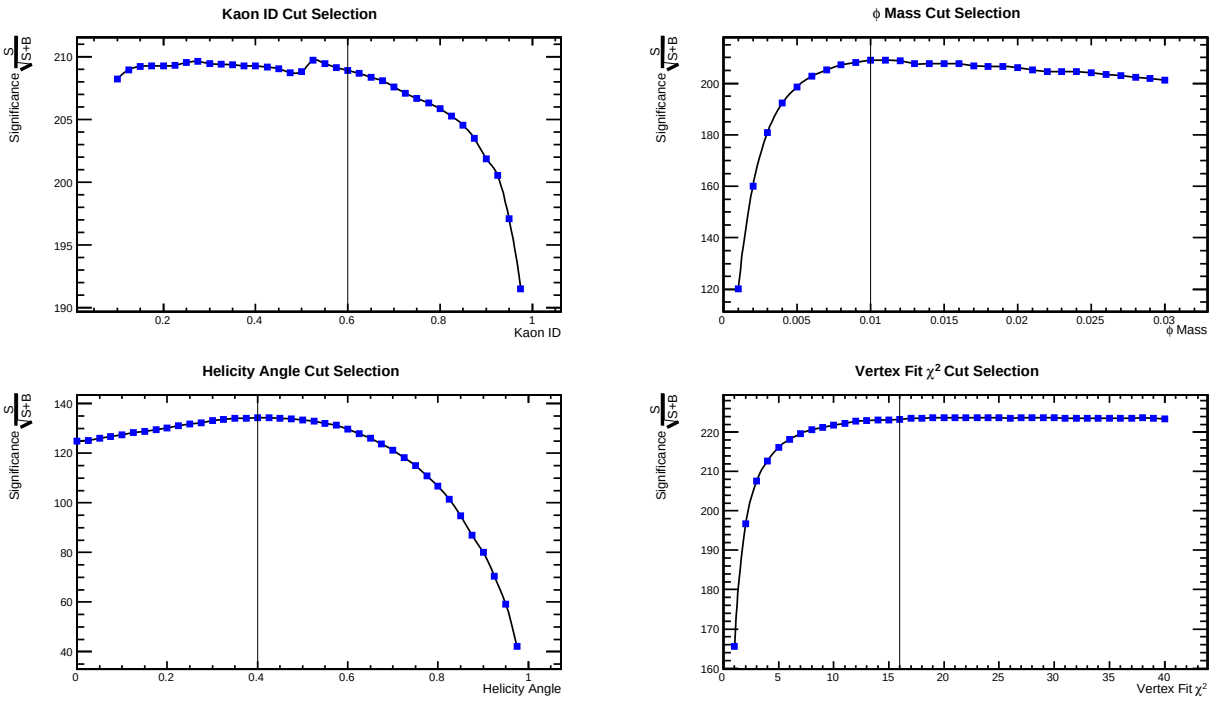

FIGURE 3.3.3: $\phi\pi$ Cut Selection Plot

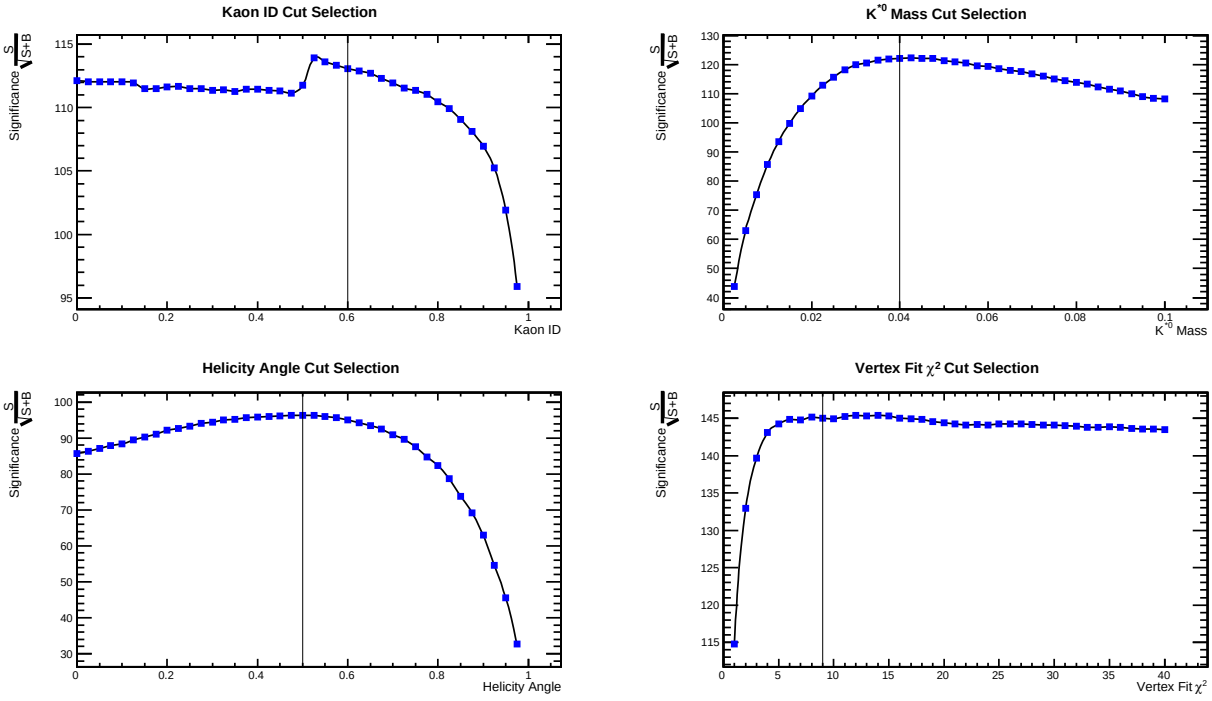

FIGURE 3.3.4: $K^{*0}K$ Cut Selection Plot

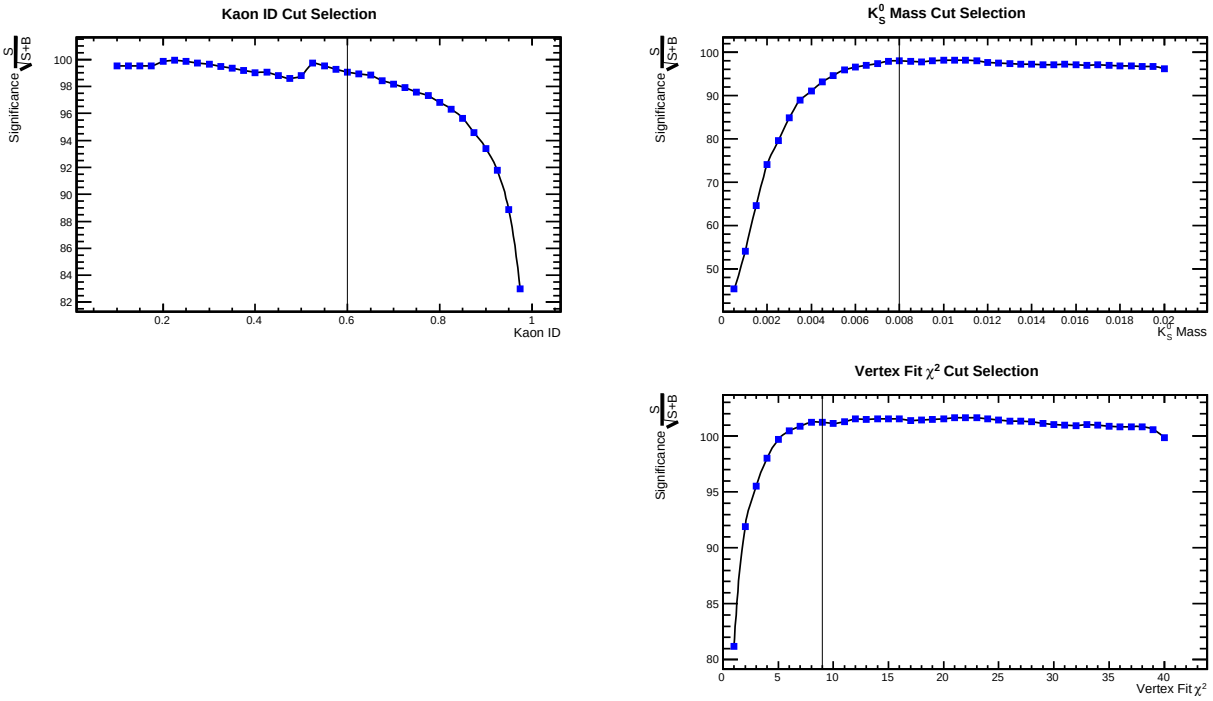

FIGURE 3.3.5: $K^0_S K$ Cut Selection Plot

3.4 D_s Momentum Spectrum

3.4.1 Reconstruction Efficiency

With the MC subsample of each decays and using the MC truth, which GenHep requirements are summarized in Table 3.4.1, the generated EvtGen momentum spectrum, can be extracted and the reconstruction efficiency ϵ_{MC} be calculated. The Figure 3.4.1, 3.4.3 and 3.4.2 give the results for the three decays.

$D_s^+ \to \phi\pi^+$	Particle ID	$D_s^- \to \phi\pi^-$	Particle ID
chgds	+1	chgds	-1
mid1	+333	mid1	+333
mid2	+333	mid2	+333
mid3	+431	mid3	−431
mmid1	+431	mmid1	−431
mmid2	+431	mmid2	−431

$D_s^+ \to \bar{K}^{*0}K^+$	Particle ID	$D_s^- \to K^{*0}K^-$	Particle ID
chgds	+1	chgds	−1
mid1	+431	mid1	−431
mid2	−313	mid2	+313
mid3	−313	mid3	+313
mmid2	+431	mmid1	−431
mmid3	+431	mmid2	−431

$D_s^+ \to K_S^0K^+$	Particle ID	$D_s^- \to K_S^0K^-$	Particle ID
chgds	+1	chgds	−1
|mid1|	+313	|mid1|	+313 [a]
mid2	+431	mid2	−431
mmid1	+431	mmid1	−431

TABLE 3.4.1: Summary of the mother ID requirements used for MC truth matching

[a] In reality, the decay is $D_s \to K^0K$ that K^0 will mix to K_S^0 or K_L^0, hence the K_S^0 can come from either K^0 or $\bar{K}^0$. In addition.

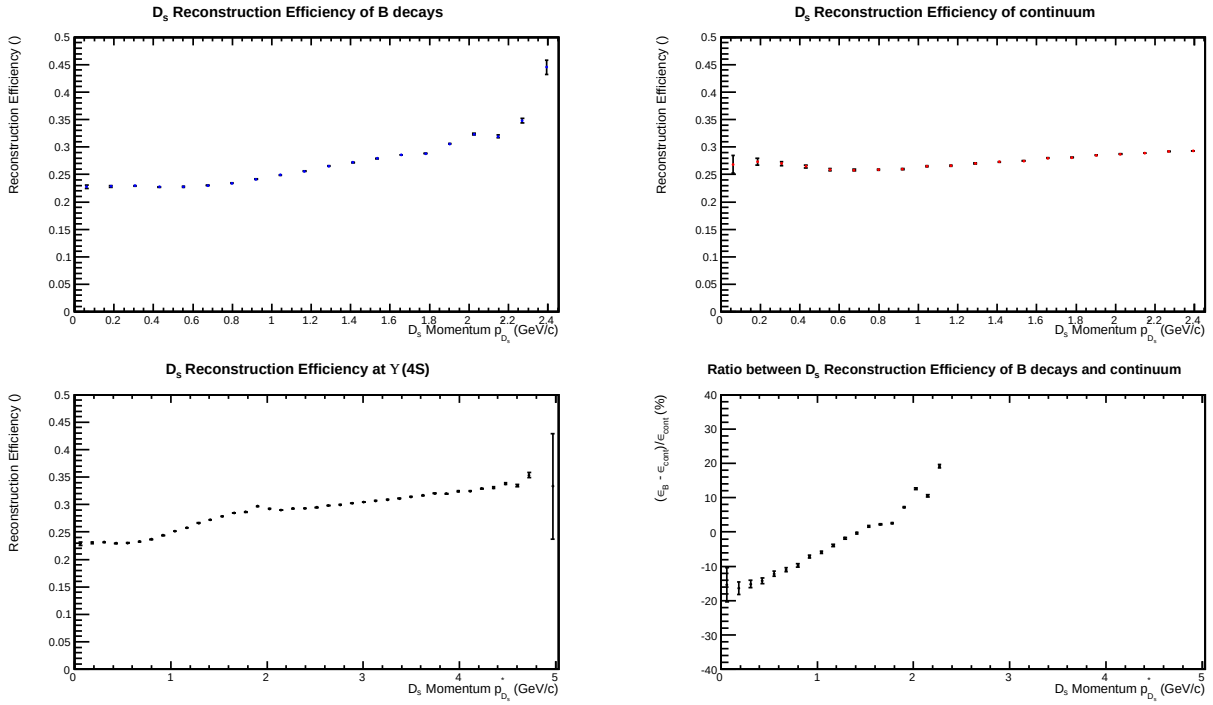

FIGURE 3.4.1: $\phi(\rightarrow K^+K^-)\pi$ Reconstruction Efficiency

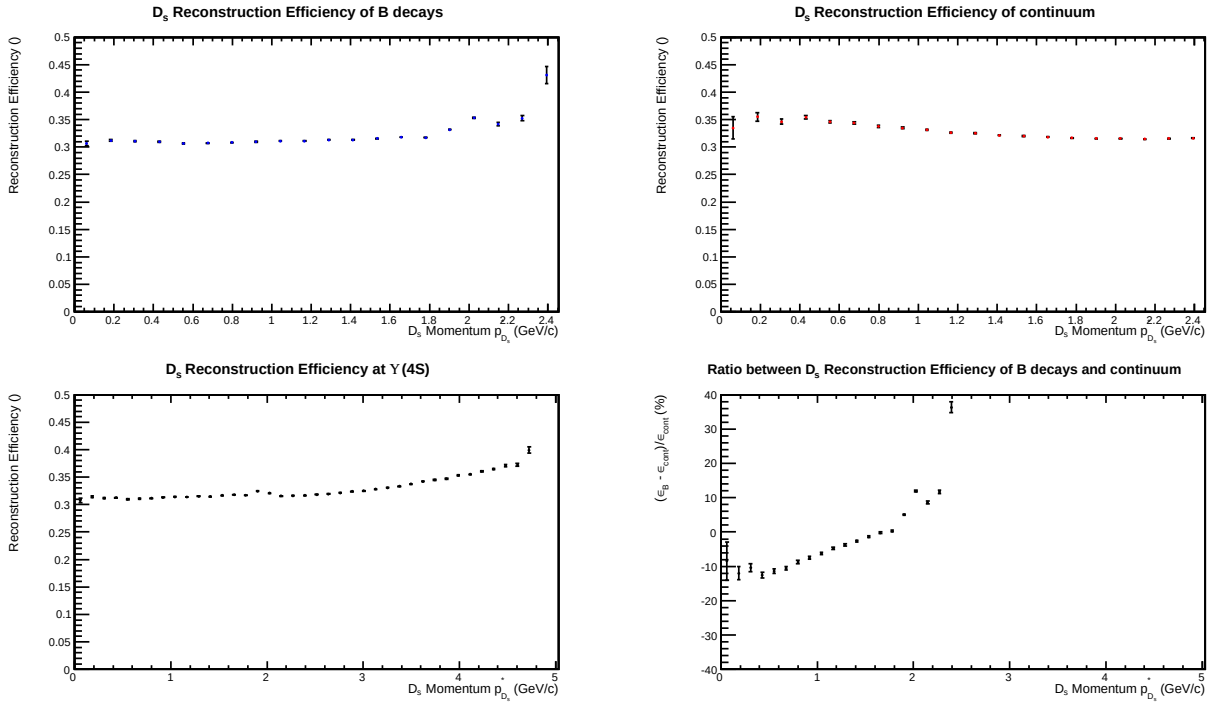

FIGURE 3.4.2: $K^0_S(\rightarrow \pi\pi)K$ Reconstruction Efficiency

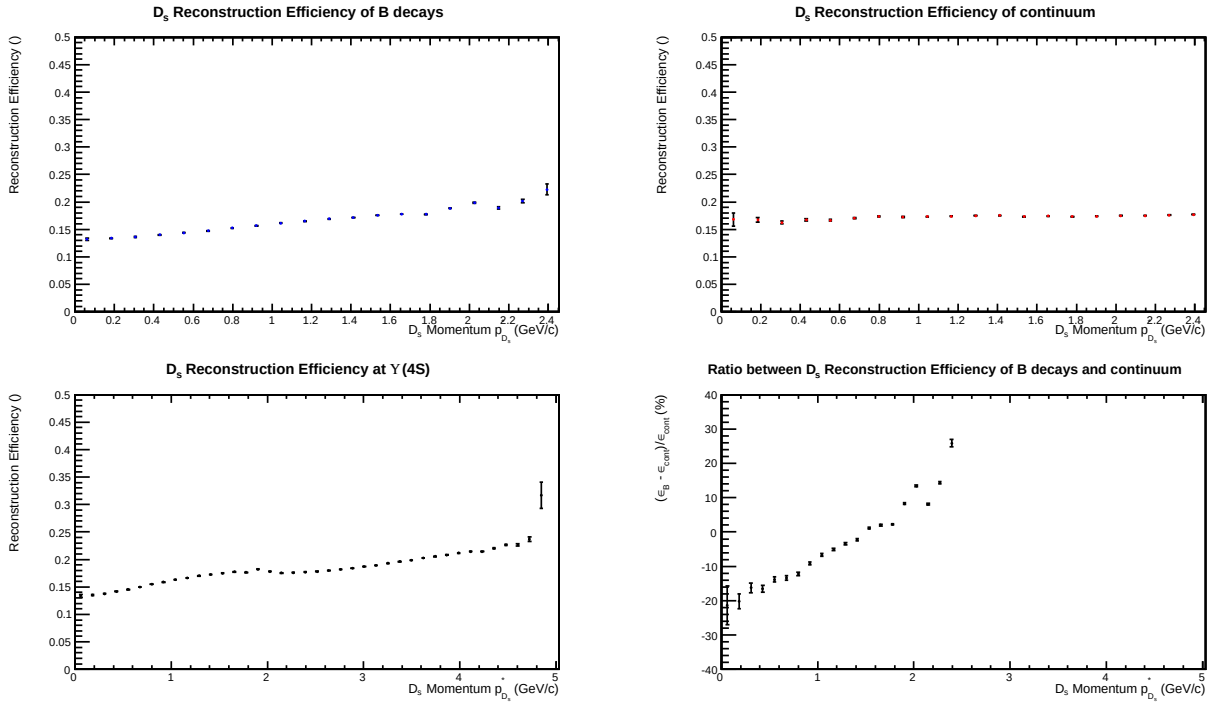

FIGURE 3.4.3: $K^{*0}(\to K\pi)K$ Reconstruction Efficiency

For the three cases, the difference in reconstruction efficiency of B decay and continuum is non zero, hence different ϵ_{MC} are used for continuum momentum spectrum scaling to $\Upsilon(4S)$ one. This can come from different angular distributions in the detector and give rise to different reconstruction efficiency. The reconstruction efficiency of $K^{*0}K$ is smaller than the two others, because a small K^{*0} mass window has been selected, compared to its large own width to suppress the large combinatorial background.

3.4.2 D_s Momentum Spectrum Extraction

D_s Mass Shape Fitting Method

Fitting the D_s mass for each momentum bin, the inclusive D_s momentum spectrum can be extracted with signal yield obtained from the procedure described in Section 3.3.4.

Figure 3.4.4 shows the fitting method results of μ, f_g, σ_1, σ_2 in bins of D_s momentum for $D_s^+ \to \phi\pi$.

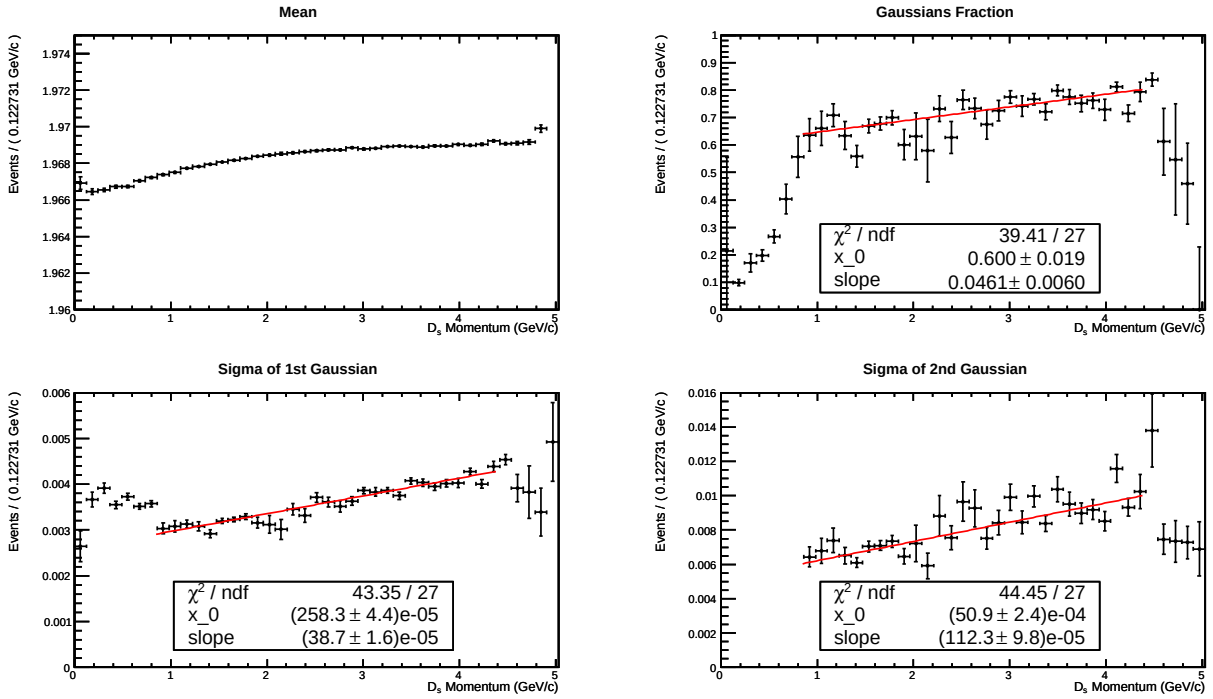

FIGURE 3.4.4: Fitting method results of μ, f_g, σ_1, σ_2 over D_s momentum for $D_s^+ \to \phi\pi^+$

As shown by these results, the fitting method with double Gaussian looks unstable in low statistics regions such as $p^*_{D_s} \in [0;0.8] \cup [2;2.2] \cup [4.3;5]$. The situation is even worse for $K^{*0}K$ and $K^0_S K$ data where purity is lower. In order to stabilize the method, a fit of the momentum dependence of the f_g, σ_1, σ_2 parameters is performed. As suggested by the results with large statistics region, a slope function is chosen. The momentum dependence of the D_s mass peak position is the subject of Appendix B.

To fix the three parameters, the following strategy is used :

1. A first fit is done in each momentum bin with user chosen seed values of μ [9], f_g, σ_1, σ_2. The μ, f_g, σ_1, σ_2 parameter values are fitted as a function of the D_s momentum with a linear function.

2. The obtained parameterizations are used as seed for second fit for better minimum finding of the mass spectrum in each momentum bin. The 1st Gaussian fraction f_g spectrum is fitted.

3. The parametrization of f_g fixes the Gaussian fraction for the next fit. After fitting, the second gaussian σ_2 spectrum is fitted.

4. f_g and σ_2 are fixed for the next fit. After fitting, the first gaussian σ_1 spectrum is fitted.

5. A final fit is performed with the three parameters fixed.

To save CPU time, this procedure is performed using binned maximum likelihood fits of the D_s mass spectrum with a bin width of 10 MeV/c^2, except for the final fits where an unbinned maximum likelihood is performed. This procedure can be used for both D_s charges together (*Simultaneous Fitting*) or separately (*Separate Fitting*).

Sidebands Fitting Method

The sidebands method become really efficient when a small signal window with most of signal yield and large sidebands for background evaluation is used. Therefore a signal window of $\approx \pm(3-4)\sigma_1$ is chosen, which gives around ± 12 MeV/c^2 and sidebands need to start far away from signal, hence at $\approx 3\sigma_2$ of the second gaussian, which is around 30 MeV/c^2, till 70 MeV/c^2, for a $\Omega_{\text{sidebands}} = 40$ MeV/c^2 sidebands width :

$$[\mu - 70; \mu - 30] \leftrightarrow [\mu - 12; \mu + 12] \leftrightarrow [\mu + 30; \mu + 70] \tag{3.10}$$

This method needs to be corrected in yield, because the tails of the mass spectrum is not taken into account. This can be done using the momentum dependent ratio $r(p^*_{D_s})$ of the fitting D_s mass shape method function between the integral around $\mu\pm$ 12 MeV/c^2 and the integral in the overall available mass region of D_s^+ and D_s^- together.

Method Comparison

Figure 3.4.5 shows the ratio between the obtained D_s yields from different methods and the MC truth yield.

The sidebands method underestimates the signal by approximately 5 % with negligible momentum dependence. For the shape fitting method, the two types of the method give consistent results between themselves, but even with two gaussian, the signal and the perhaps background shapes seam more complicated, therefore a more advanced PDF shape would be needed for better precision. The ratio of the corrected sidebands method gives the best results for the D_s yield extraction with an underestimation of (-1.3 ± 0.3) % (the ratio is weighted with the MC truth D_s yield of each bin) for $\phi\pi$ which will be assign to systematics. Therefore the best method for the inclusive branching fraction is the corrected sidebands method. Further studies are needed to extracted the bias created by the method for $K^{*0}K$ and $K^0_S K$.

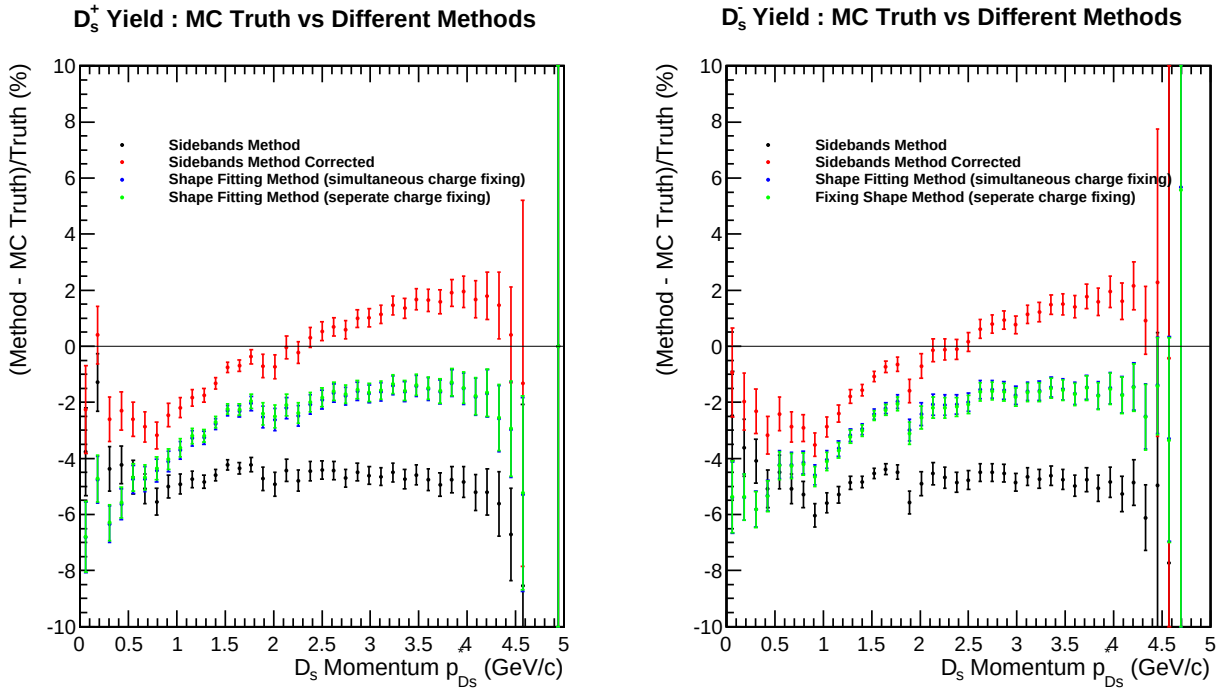

FIGURE 3.4.5: Ratio between different yield extraction methods and the MC truth with $D_s \to \phi\pi$

3.4.3 Inclusive Branching Fraction of $\mathcal{B}(B \to D_s X)$

Generic MC

Figure 3.4.6 shows the MC reconstructed D_s momentum spectrum at $\Upsilon(4S)$ resonance.

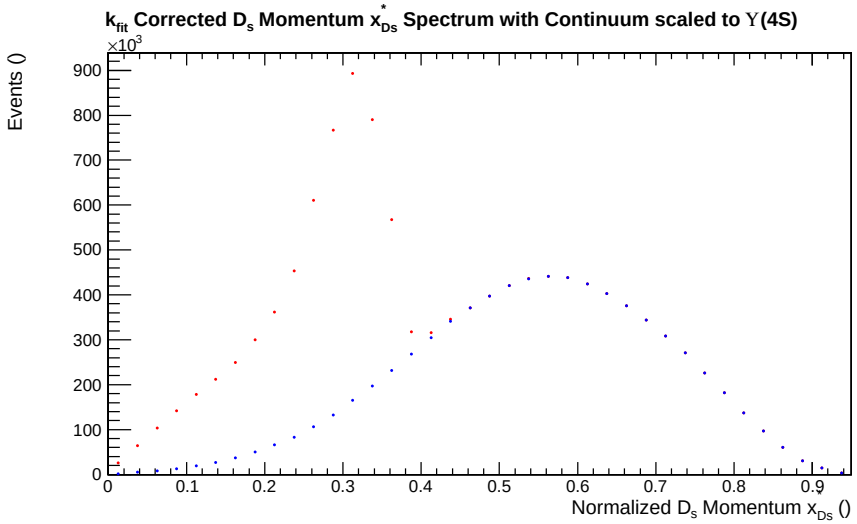

FIGURE 3.4.6: MC reconstructed D_s momentum spectrum at $\Upsilon(4S)$

To check the method and the software procedure, the same script than data is used for $\phi\pi$. Table 3.4.2 shows the results of the extracted product of branching fractions compared to the branching fractions product from the Belle decay tables used for MC generation. The number of $\Upsilon(4S)$ generated events is needed ($N_{B\bar{B}}$), therefore a script has been developed to count the number of generated $B\bar{B}$ pairs recorded in log files.

	$\mathcal{B}(B \to D_s^{\pm} X) \cdot \mathcal{B}(D_s \to \phi\pi) \cdot \mathcal{B}(\phi \to K^+K^-)$
Generated	$(0.195)\,\%$ [a]
Reconstructed	$(0.191 \pm 0.001\,^{+0.003}_{-0.000})\,\%$ [b]

TABLE 3.4.2: Generated and Reconstructed $\mathcal{B}(B \to D_s^{\pm} X) \cdot \mathcal{B}(D_s \to \phi\pi) \cdot \mathcal{B}(\phi \to K^+K^-)$

[a] the number of $B \to D_s(\to \phi(\to K^+K^-)\pi)X$ has been obtained from the number of entries in $\phi\pi$ channel GenHep ntuple (`chds` $= 1$)

[b] the systematic error stands for bias between corrected sidebands method yield and MC truth one

The results are in good agreement with each other, which means that the method works.

Data

Using the same script than the MC one, Figure 3.4.7, 3.4.8 and 3.4.9 show the data results of the normalized D_s momentum $x^*_{D_s}$ for $\Upsilon(4S)$ and continuum data, the superposition of the $\Upsilon(4S)$ and k_{fit} scaled continuum spectrum and the efficiency corrected subtracted spectrum. The scaled factor k_{fit} for continuum scaling has been obtained from a constant fit of the ratio between $\Upsilon(4S)$ and continuum momentum spectrum. Looking at the data and MC spectrum, the proportion of continuum and B decay in the two samples are not consistent. Therefor, evaluating the reconstruction efficiency at $\Upsilon(4S)$ can present a biais because calculated according to B decay and continuum yields. Then, the method has been changed and only the

substracted spectrum is efficiency corrected using B decay reconstruction efficiency, which does not present a biais due to B decay over continuum yield ratio. The new formula for expected B events is given by :

$$N_{exp}^{B} = \sum_{x_p^*} \frac{1}{\epsilon^B(x_p^*)} \left(N_{reco}^{\Upsilon(4S)}(x_p^*) - N_{reco}^{cont}(x_p^*) \cdot \frac{\mathcal{L}_{\Upsilon(4S)}}{\mathcal{L}_{cont}} \cdot \frac{E_{cont}^2}{E_{\Upsilon(4S)}^2} \right) \tag{3.11}$$

where ϵ^B is the reconstruction efficiency of B decay events.

Table 3.4.1 summarize the data results of the expected D_s yield, the inclusive branching fraction $\mathcal{B}(B \to D_s^{\pm} X) \cdot \mathcal{B}(B \to i)$, the scale factor between $\Upsilon(4S)$ spectrum and continuum one and the expected scale factor k_{exp} given by $k_{exp} = \frac{\mathcal{L}_{\Upsilon(4S)}}{\mathcal{L}_{cont}} \cdot \frac{E_{cont}^2}{E_{\Upsilon(4S)}^2}$ for cross-check.

i	k_{fit}	k_{exp}	N_{reco}/ϵ_{MC}	$\mathcal{B}(B \to D_s^{\pm} X) \cdot \mathcal{B}(B \to i)$
$\phi(\to K^+K^-)\,\pi$	8.47 ± 0.04	$8.77 \pm 0.17 \pm 0.09^a$	$(3.3311 \pm 0.0055) \cdot 10^6$	$(0.2159 \pm 0.0015)\,\%$
$K^{*0}(\to K\pi)\,K$	8.44 ± 0.04	$8.77 \pm 0.17 \pm 0.09$	$(4.8442 \pm 0.0136) \cdot 10^6$	$(0.3129 \pm 0.0023)\,\%$
$K_S(\to \pi^+\pi^-)K$	8.35 ± 0.06	$8.77 \pm 0.17 \pm 0.09$	$(1.7425 \pm 0.0061) \cdot 10^6$	$(0.1129 \pm 0.0009)\,\%$

TABLE 3.4.3: Fitted data scale factor k_{fit}, expected scale factor k_{exp}, expected generated events N_{reco}/ϵ_{MC} and branching fraction product $\mathcal{B}(B \to D_s^{\pm} X) \cdot \mathcal{B}(B \to i)$

[a] where the first error is statistical from integrated luminosities error of 1.4 % and the second for systematical error on the on_resonance over continuum integrated luminosity ratio

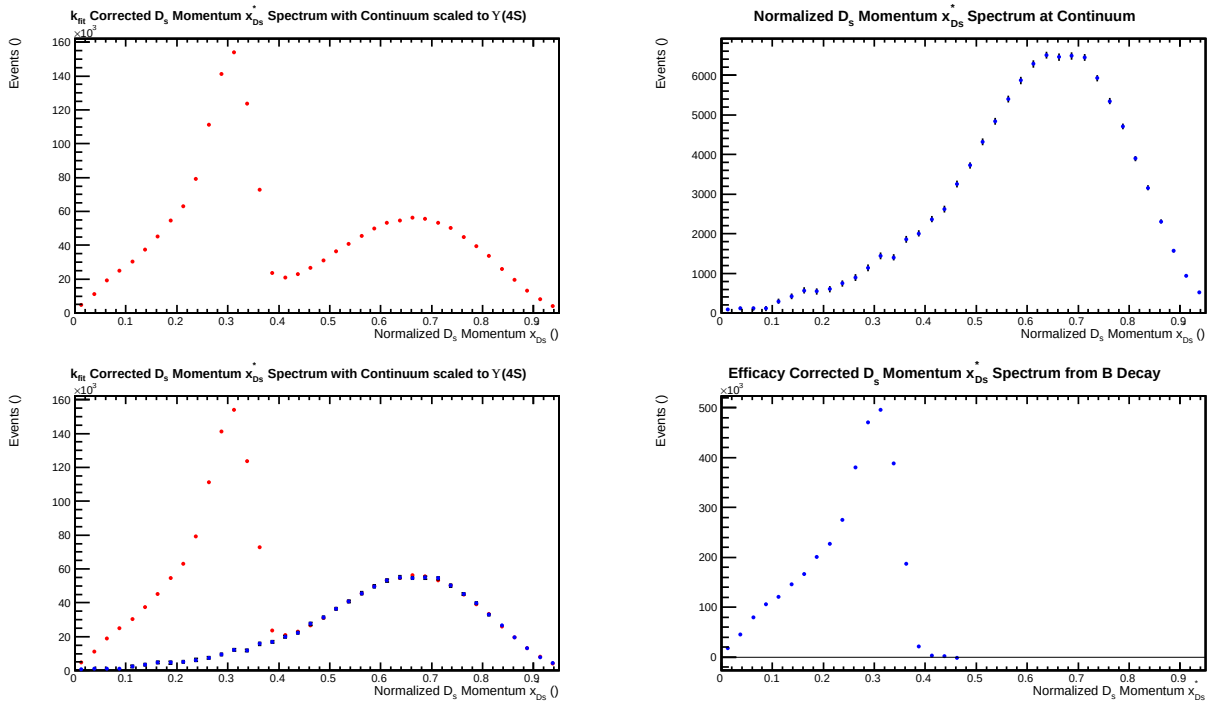

FIGURE 3.4.7: $\phi\pi$ Data D_s momentum spectrum. *Up left* : $\Upsilon(4S)$ spectrum. *Up right* : Continuum spectrum. *Down left* : Continuum to $\Upsilon(4S)$ data scaled spectrum *Down right* : Subtracted spectrum

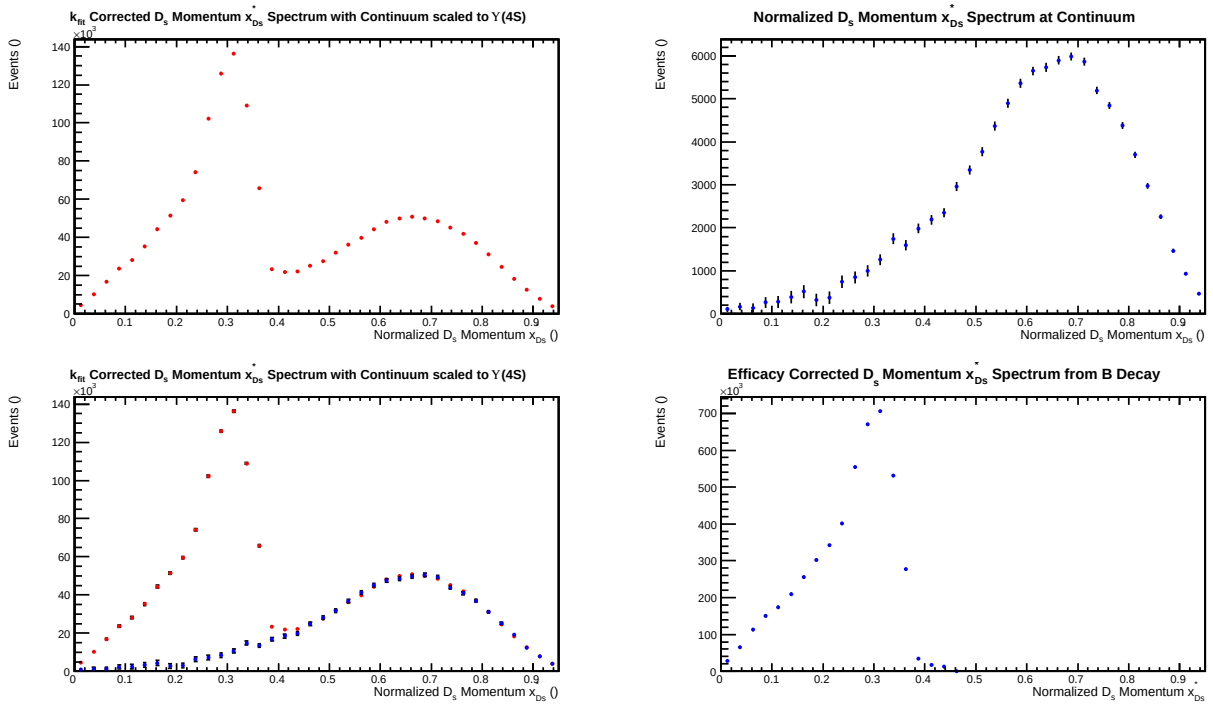

FIGURE 3.4.8: $K^{*0}K$ Data D_s momentum spectrum. *Up left* : $\Upsilon(4S)$ spectrum. *Up right* : Continuum spectrum. *Down left* : Continuum to $\Upsilon(4S)$ data scaled spectrum *Down right* : Subtracted spectrum

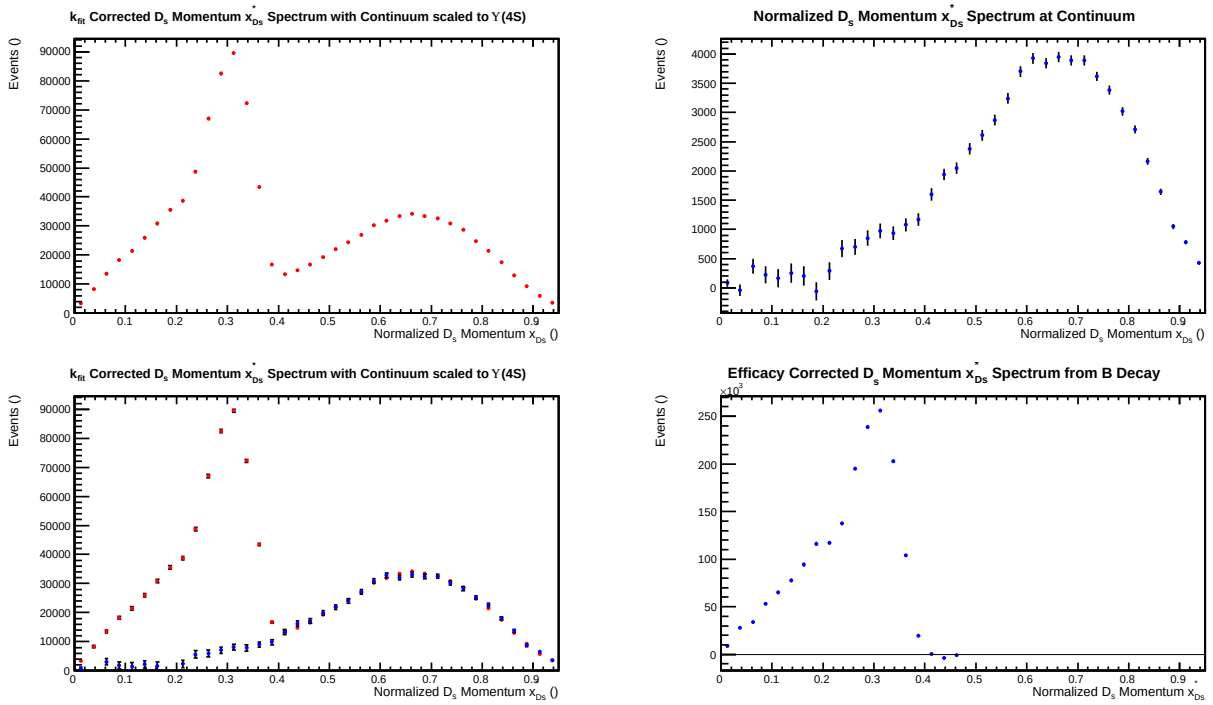

FIGURE 3.4.9: $K^0_S K$ Data D_s momentum spectrum. *Up left* : $\Upsilon(4S)$ spectrum. *Up right* : Continuum spectrum. *Down left* : Continuum to $\Upsilon(4S)$ data scaled spectrum *Down right* : Subtracted spectrum

The results for the fitted scale factor and expected one do not coincide. The first possibility comes from some non expected variation of the BhaBha efficiency which is the channel to measure integrated luminosity. And second, the dependence on energy of the hadronic cross-section can be more complicated than E^{-2}.

Assuming branching fractions of the D_s decay modes given by the PDG [9], the inclusive branching fraction $\mathcal{B}(B \to D_s^{\pm} X)$ for each of the decay modes can be computed. The preliminary results are :

$$\mathcal{B}(B \to D_s^{\pm} X) = (10.06 \pm 0.07(\text{stat}) \pm 0.79(\mathcal{B}))\,\% \cdot \frac{\mathcal{B}(D_s \to \phi\,\pi)}{(4.39 \pm 0.34)\,\%} \cdot \frac{\mathcal{B}(\phi \to K^+K^-)}{(48.9 \pm 0.5)\,\%} \tag{3.12}$$

$$\mathcal{B}(B \to D_s^{\pm} X) = (12.07 \pm 0.09(\text{stat}) \pm 1.86(\mathcal{B}))\,\% \cdot \frac{\mathcal{B}(D_s \to K^{*0}(\to K\pi)\,K)}{(2.6 \pm 0.4)\,\%} \tag{3.13}$$

$$\mathcal{B}(B \to D_s^{\pm} X) = (10.95 \pm 0.08(\text{stat}) \pm 0.67(\mathcal{B}))\,\% \cdot \frac{\mathcal{B}(D_s \to K_S^0\,K)}{(1.49 \pm 0.09)\,\%} \cdot \frac{\mathcal{B}(K_S^0 \to \pi^+\pi^-)}{(69.20 \pm 0.05)\,\%} \tag{3.14}$$

where first error is statistical and second one is induced by the D_s branching fractions. The PDG value for the inclusive branching fraction is $\mathcal{B}(B \to D_s^{\pm} X) = (8.4 \pm 0.8)\,\%$ [9].

The obtained results are in agreement with each other according to the large error on D_s branching fractions. But a possible peaking background of non resonant D_s , $D_s \to K^+K^-\pi$ decay needs to be subtracted. Therefore these results are overestimated and more studies are needed. But still, for K_SK decay, the K_S is well reconstructed, due to its macroscopic flight distance, therefore the peaking background must be very small, then the correction to these results should be small. For $\phi\pi$, the peaking background is expected to be less than 1 %, because the ϕ resonance is a narrow $K\bar{K}$ threshold resonance and its non resonant background under signal is small, due to small phase space available. But some non negligible peaking background is possible for $K^{*0}K$ decay which is consistent with the larger branching fraction obtained using $K^{*0}K$ than $\phi\pi$ and K_SK one.

In addition, all the systematics, except from the method one, need be done afterwards.

Extracting the error not coming from $D_s \to \phi\pi$ branching fraction knowledge of PDG value and with a systematic error of 1 % due to peaking background, the ratio between obtained result and PDG one gives :

$$\frac{\mathcal{B}(B \to D_s^{\pm} X)_{\text{exp}}}{\mathcal{B}(B \to D_s^{\pm} X)_{\text{PDG}}} = \frac{(10.06 \pm 0.07\,(\text{stat}) \pm 0.10\,(\text{non res}))\,\%}{(8.4 \pm 0.5)\,\%} = 1.20 \pm 0.07 \tag{3.15}$$

which gives before other systematics evaluation, a 3σ difference measurement.

Non resonant background in $D_s \to \phi\pi$ estimation

Looking at the K^+K^- invariant mass spectrum (see Figure 3.4.10), the contribution from $D_s \to K^+K^-\pi$ has phase space distribution. Each part of the spectrum can be approximate by a square-root function. Therefore the $D_s \to K^+K^-\pi$ yield is proportional to :

$$N_{\Omega_{all}}^{\text{non res}} \propto 2 \cdot \int_{\Omega_{all}/2} \sqrt{m_{KK} - 2 \cdot m_K}\; dm_{KK} = 2 \cdot \{m_{KK} - 2 \cdot m_K\}^{3/2}\Big|_{\Omega_{all}/2} \tag{3.16}$$

Then, the proportion of $D_s \to K^+K^-\pi$ events in ϕ mass signal window can be calculated as :

$$\frac{N_{\Omega_{sig}}^{\text{non res}}}{N_{\Omega_{all}}^{\text{non res}}} = \frac{\{m_{KK} - 2 \cdot m_K\}^{3/2}\Big|_{\Omega_{sig}}}{2 \cdot \{m_{KK} - 2 \cdot m_K\}^{3/2}\Big|_{\Omega_{all}/2}} = 0.98\,\% \approx 1\,\% \tag{3.17}$$

where the signal window is $\Omega_{sig} = 2 \cdot m_K + m_\phi \pm 10\,\text{MeV/c}^2$ and $\Omega_{all} = [2 \cdot m_K; m_{D_s} - m_\pi]$ [9].

Finally, the contribution of non resonant background in D_s mass window is proportional to the branching fractions ratio of $D_s \to K^+K^-\pi$ and $D_s \to \phi\pi$, which gives the following estimation :

$$\frac{N_{\Omega_{sig}}^{\text{non res}}}{N_{\Omega_{sig}}^{\phi\pi}} = \frac{N_{\Omega_{sig}}^{\text{non res}}}{N_{\Omega_{all}}^{\text{non res}}} \cdot \frac{\mathcal{B}(D_s \to K^+K^-\pi \text{ non res})}{\mathcal{B}(D_s \to \phi\pi)} < 1\% \tag{3.18}$$

where the branching fractions ratio is expected to be less than 1, even the non resonant branching fraction has never been measured.

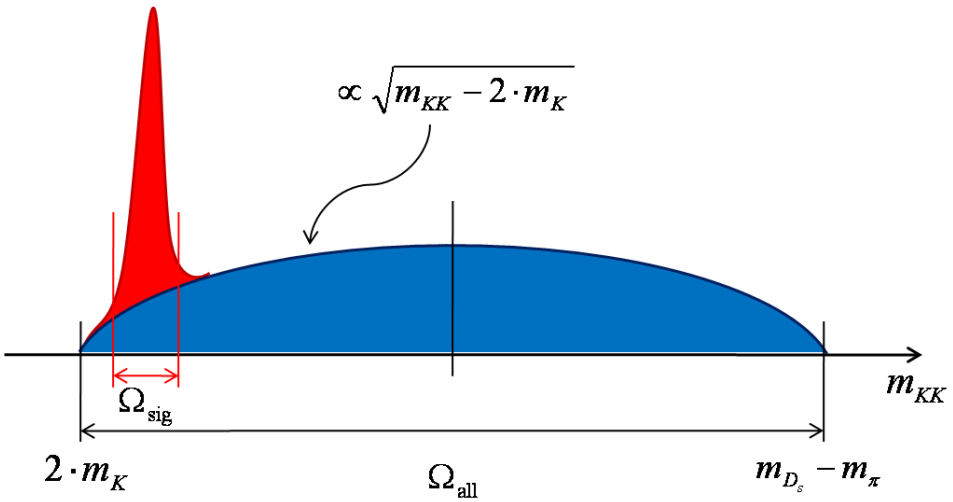

FIGURE 3.4.10: KK invariant mass spectrum with in red ϕ resonnance and in blue the non resonant background from $D_s \to K^+K^-\pi$.

Chapter 4

Direct CP Violation in $B \to D_s^{(*)} D^{(*)}$

4.1 DCPV in $B \to D_s^{(*)} D^{(*)}$ extraction method using partial reconstruction technique

Using a partial reconstruction technique reconstructing only the D_s, only the sum of the asymmetries of $B \to D_s^{(*)} D^{(*)}$ is accessible. Even, with the sum, results can still give interesting and important conclusions.

4.1.1 Other charge asymmetries phenomena

In the case of zero or non zero asymmetry in $B \to D_s^{(*)} D^{(*)}$ momentum window, there is still other possible phenomena that can lead to these results :

- *Detector Asymmetry* : The particle and its antiparticle can behave differently in the detector, their interaction cross sections with matter can be different. There is a low momentum example that is the *pionic capture* case, where a pion π^- takes the electron place around the nucleus and the anti-pion π^+ cannot. There are many cases where qq and $q\bar{q}$ interactions can lead to possible non negligible cross section differences. Hence a *charge asymmetry*, the yield difference between particles and antiparticles, can emerged. In addition, possible differences can appear when proceeding the momentum evaluation. If the dE/dx difference is not well known between the particle and its antiparticle, the particle momentum can be wrongly evaluated from the helix parametrization of the tracks, where dE/dx is strongly involved (see 2.4). This could lead to a momentum shift and give rise to a charge asymmetry where the D_s momentum spectrum varies strongly like in $[1.8; 2.0]$ GeV/c^2 region.
- *DCPV in D_s decays* : In addition to detection asymmetries of the D_s decay products, there is still known or unknown DCPV in chosen D_s decays that have to be taken into account.

The sum of these two asymmetries can be extracted from the pure continuum region where no B decay is involved. The asymmetry extraction can be done using a constant or more advanced function depending on the results because these asymmetries could be momentum dependent.

4.1.2 DCPV in $B \to D_s^{(*)} D^{(*)}$ extraction technique

For DCPV extraction in $B \to D_s^{(*)} D^{(*)}$, the other possible asymmetries have to be taken into account. In the assumption that the possible detector asymmetry is the same for B decay event and continuum ones, the asymmetries are small, the measured charge asymmetry in $B \to D_s^{(*)} D^{(*)}$ momentum region can be factorized :

$$\mathcal{A}_{obs} \approx \mathcal{A}_{det} + \mathcal{A}_{D_s} + \mathcal{A}_B \tag{4.1}$$

where $\mathcal{A}_{obs} = \frac{N^+_{reco} - N^-_{reco}}{N^+_{reco} + N^-_{reco}}$ is the observed charge asymmetry, $\mathcal{A}_{det} = \frac{\epsilon^+ - \epsilon^-}{\epsilon^+ + \epsilon^-}$ the detector asymmetry with $\epsilon^\pm$ the *reconstruction efficiency* (ratio between reconstructed events in MC Truth (see 3.3.2) and generated events yield), $\mathcal{A}_{D_s} + \mathcal{A}_B = \frac{N^+_{gen} - N^-_{gen}}{N^+_{gen} + N^-_{gen}}$ the DCPV asymmetry from B and D_s decay. The $N^\pm_{obs}$ observed $D^\pm_s$ yield can be written as $N^\pm_{obs} = \epsilon^\pm \cdot N^\pm_{gen}$ using the reconstruction efficacies. Then :

$$\mathcal{A}_{obs} = \frac{N^+_{reco} - N^-_{reco}}{N^+_{reco} + N^-_{reco}} = \frac{\epsilon^+ \cdot N^+_{gen} - \epsilon^- \cdot N^-_{gen}}{\epsilon^+ \cdot N^+_{gen} + \epsilon^- \cdot N^-_{gen}} \tag{4.2}$$

The $N^\pm_{gen}$ and $\epsilon^\pm$ can be written as $N^\pm_{gen} = \bar{N}_{gen}(1 \pm \mathcal{A}_{DCPV})$ and $\epsilon^\pm = \bar{\epsilon}(1 \pm \mathcal{A}_{det})$ where $\bar{N}_{gen} = \frac{N^+_{gen} + N^-_{gen}}{2}$ and $\bar{\epsilon} = \frac{\epsilon^+_{gen} + \epsilon^-_{gen}}{2}$. Then $\mathcal{A}_{obs}$ can be rewritten as :

$$\mathcal{A}_{obs} = \frac{(1 + \mathcal{A}_{det}) \cdot (1 + \mathcal{A}_{DCPV}) - (1 - \mathcal{A}_{det}) \cdot (1 - \mathcal{A}_{DCPV})}{(1 + \mathcal{A}_{det}) \cdot (1 + \mathcal{A}_{DCPV}) + (1 - \mathcal{A}_{det}) \cdot (1 - \mathcal{A}_{DCPV})} = \mathcal{A}_{DCPV} + \mathcal{A}_{det} + \mathcal{O}(\mathcal{A}_{DCPV} \cdot \mathcal{A}_{det}) \tag{4.3}$$

Which gives with $\mathcal{A}_{DCPV} = \mathcal{A}_B + \mathcal{A}_{D_s}$, the following observed asymmetry $\mathcal{A}_{obs}$:

$$\mathcal{A}_{obs} = \mathcal{A}_{det} + \mathcal{A}_{D_s} + \mathcal{A}_B + \mathcal{O}[(\mathcal{A}_B + \mathcal{A}_{D_s}) \cdot \mathcal{A}_{det}] \approx \mathcal{A}_{det} + \mathcal{A}_{D_s} + \mathcal{A}_B \tag{4.4}$$

under the assumption that $\mathcal{A}_{det,D_s,B} << 1$. Finally, the $B \to D_s^{(*)} D^{(*)}$ can be obtained as :

$$\mathcal{A}_B \approx \mathcal{A}_{obs} - (\mathcal{A}_{det} + \mathcal{A}_{D_s}) = \mathcal{A}_{obs} - \mathcal{A}_{cont} \tag{4.5}$$

where $\mathcal{A}_{cont}$ is the asymmetry obtained from the pure continuum part [1].

4.1.3 Possible outcomes of DCPV search in $B \to D_s^{(*)} D^{(*)}$

- *DCPV in* $B \to D_s^{(*)} D^{(*)}$: There exists at least a DCPV in one of the eight possible asymmetries. If the DCPV is too large to fit to SM predictions, possible new physics can be found.
- *no DCPV in* $B \to D_s^{(*)} D^{(*)}$: Then, no clear conclusions can emerge, because only the sum of the eight asymmetries is found and compensations of these asymmetries are possible. But this result can still restrict some DCPV predictions of SM and new physics models.

[1] under the assumption that the continuum asymmetry on B decay is the same than pure continuum part

4.2 Generic MC

To extract the charge asymmetry, the methods need to be tested with MC. Table 4.2.1 summarizes all the DCPV fit results with $\phi\pi$ (the other final states will be done afterwards).

	B decays region	Pure continuum region
Fit Window	$1.4 < p^*_{D_s} < 2$	$2.5 < p^*_{D_s} < 4.5$
Charged/mixed GenHep	$(-0.031 \pm 0.027)\,\%$	-
Udsc GenHep	$(-0.027 \pm 0.053)\,\%$	$(-0.012 \pm 0.026)\,\%$
Charged/mixed MC Truth	$(-0.48 \pm 0.07)\,\%$	-
Udsc MC Truth	$(-0.49 \pm 0.07)\,\%$	$(-0.32 \pm 0.05)\,\%$
Sidebands $\Upsilon(4S)$	$(-0.38 \pm 0.06)\,\%$	$(-0.28 \pm 0.05)\,\%$
Fitting $\Upsilon(4S)$	$(-0.47 \pm 0.05)\,\%$	$(-0.33 \pm 0.05)\,\%$

TABLE 4.2.1: DCPV fit results on MC in GenHep, MC Truth, with Sidebands and Together fitting methods in B decays region ($1.4 < p^*_{D_s} < 2$) and pure continuum region($2.5 < p^*_{D_s} < 4.5$) (see Figure 4.2.2)

The first step is to fit the GenHep spectrum to search for implemented DCPV at the generation level. Looking at the GenHep results, no DCPV is found, as expected since no DCPV has been discovered neither in $B \to D_s^{(*)} D^{(*)}$, in $D_s \to \phi\pi$ or in $e^+e^- \to D_s^+ D_s^-$. The next step is to look for DCPV in the reconstructed D_s spectrum in the MC truth. First, there is in the MC a DCPV like shown by the results, which means that there exists a detector asymmetry. The fit for udsc and charged/mixed are compatible, but there is a non zero difference between DCPV in low momentum and high momentum region. It means that there is a momentum-dependent detector asymmetry. Therefore, the assumption of same detector asymmetry in B region and pure continuum region presents a bias. A fit with a slope function has been tested but the fit is unstable and gives bad results. Then, this assumption bias will be added to the systematics.

The last two plots of Figure 4.2.1 present the results with simultaneous D_s mass fitting and sidebands method. The simultaneous fitting method is chosen because has less statistical fluctuations than separate fitting method because of common parameterizations, double statistics, and the results are closer to MC results. In addition, possible charge asymmetry created by two different parameterizations is avoided. The fit in the pure continuum part gives results in agreement with the MC truth. Same for the fit in B region. To take into account the bias created by the same DCPV assumption in pure continuum and B region, $(+0.16 \pm 0.09)\,\%$ will be added to data systematics. In addition, the bias created by the method in the B region will be assigned to data systematics.

The simultaneous fitting method is chosen for data because is closer to MC truth results than sidebands method.

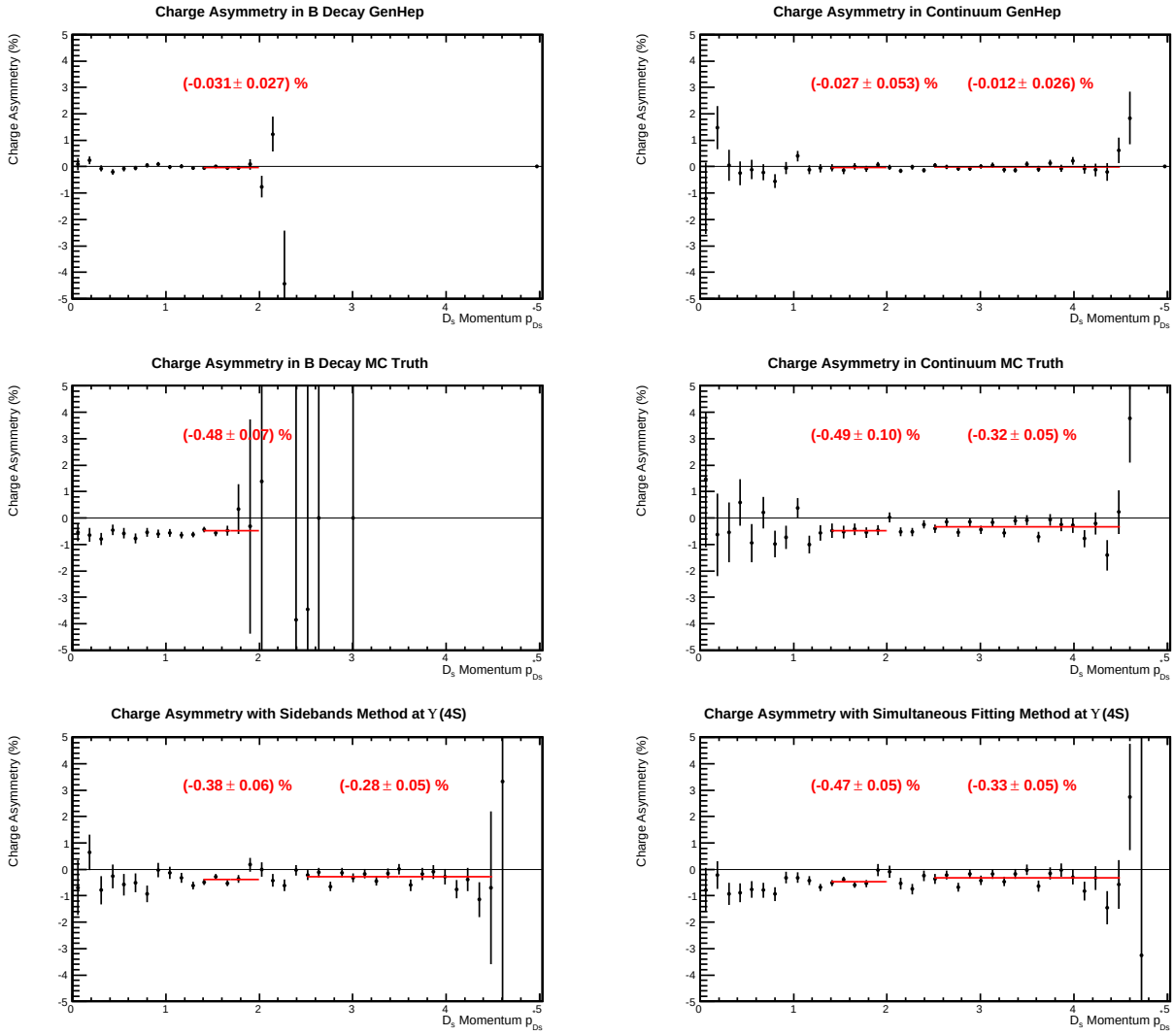

FIGURE 4.2.1: MC DCPV fit results plots of GenHep, MC Truth, with Sidebands and Simultaneous fitting methods

4.3 Data

The Figure 4.3.1 shows the data results of the procedure tested on MC.

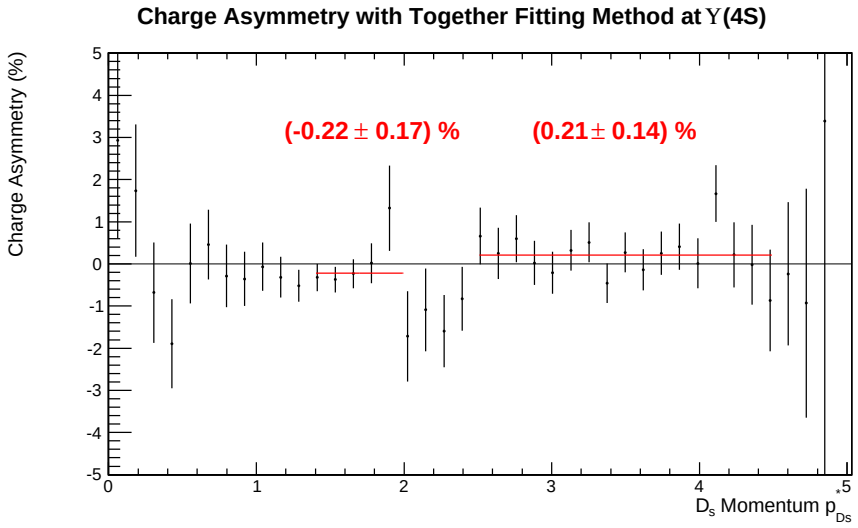

FIGURE 4.3.1: Data DCPV fit results plots with *Up*, the pure continuum and *Down*, the corrected asymmetry fit spectrum with fit of $B \to D_s^{(*)} D^{(*)}$ decay region

The fit in the B region gives the following DCPV in $B \to D_s^{(*)} D^{(*)}$ decays :

	Simultaneous Fitting D_s Shape Method
$\mathcal{A}_{CP}(B \to D_s^{(*)} D^{(*)})$	$(-0.43 \pm 0.22\ ^{+0.16}_{-0.02})\ \%$

TABLE 4.3.1: Summary of DCPV in $\mathcal{A}_{CP}(B \to D_s^{(*)} D^{(*)})$ with Sidebands and Simultaneous fitting method

The results are compatible with zero DCPV in $B \to D_s^{(*)} D^{(*)}$ with partial reconstruction technique and large Belle data sample. But there is an interesting behavior in $2 < p^*_{D_s} < 2.4$ region spectrum coming from $B \to D_s h$ decays where h stands for light mesons. More deep studies are needed.

Chapter 5

Conclusion

Reconstructing the D_s meson with three clean decay modes, preliminary results before peaking background subtraction of the inclusive branching fraction of $B \to D_s^{\pm} X$ has been obtained with the help of a corrected sidebands method. The result with $D_s \to \phi\pi$ is the following with the full $\Upsilon(4S)$ data sample of 710 fb^{-1} :

$$\mathcal{B}(B \to D_s^{\pm} X) \quad = \quad (10.06 \pm 0.07(\text{stat}) \pm 0.79(\mathcal{B}))\,\% \cdot \frac{\mathcal{B}(D_s \to \phi\,\pi)}{(4.39 \pm 0.34)\,\%} \cdot \frac{\mathcal{B}(\phi \to K^+K^-)}{(48.9 \pm 0.5)\,\%}$$

with a peaking background estimated to be less than 1 %. Without other systematics evaluation, a 3σ difference to the PDG value has been found.

With systematics computation and peaking background subtraction, a precise measurement of the inclusive branching fraction $\mathcal{B}(B \to D_s^{\pm} X)$ can be obtained and ratios of $K^{*0}K$ and $K_S K$ to the $\phi\pi$ branching fraction can be extracted.

A compatible with zero DCPV in $B \to D_s^{(*)} D^{(*)}$ of $(-0.43 \pm 0.22\ ^{+0.16}_{-0.02})\,\%$ has been obtained.

With the help of the fitting method mean μ parameter, preliminary results show a momentum dependence of the D_s mass peak position. Further studies are needed.

Finally, the invisibility of the $\Upsilon(5S) \to \Upsilon(4S)\,\pi^+\,\pi^-$ decay at Belle has been claimed due to huge combinatorial background and no strong cuts finding.

Appendix A

Search for $\Upsilon(5S) \rightarrow \Upsilon(4S)\ \pi^+\ \pi^-$

A.1 Introduction

The $\Upsilon(5S)$ has been discovered by CLEO [17] and CUSB [18] in 1985. The PDG average of these 2 experiments for the mass is 10.865 ± 0.008 GeV and for the width is 110 ± 13 MeV [**?**].

Recently, plenty of charmonium-like mesons has been discovered with the use of the B factories. Lots of them are in agreement with the charmonium spectroscopy. But, there are a number of new resonances like the X(3872) and Y(4260) that not seem to fit in the $c\bar{c}$ spectrum. The interpretation of these states should be beyond the well-known mesons and baryons. From the QCD theory, possible new bound states would be, for example, an hybrid state $[c\bar{c}g]$, a thetraquark state $[c\bar{c}q\bar{q}]$ or a molecular structure $[c\bar{q} - \bar{c}q]$.

In recent publications, the decay $\Upsilon(5S) \rightarrow \Upsilon(nS)\pi^+\pi^-$ has been observed by the Belle Collaboration for n=1,2,3 [19]. This decay has been reconstructed exclusively using the electromagnetic decay $\Upsilon(nS) \rightarrow \mu^+\mu^-$ and the charged pions for n=1,2,3. In addition, they reported an anomalous in the $\Upsilon(5S) \rightarrow \Upsilon(nS)\pi^+\pi^-$ production. First, a partial width for the previous decay has been measured, near the $\Upsilon(5S)$ resonance, with two orders of magnitude bigger than the less energetic $\Upsilon(nS)$ mesons [19]. And secondly, using a scan sample between 10.83 GeV and 11.02, an enhancement of the $\Upsilon(nS)\pi^+\pi^-$ production, with a maximum which is shifted compared to the world average $\Upsilon(5S)$ mass, has been observed for n=1,2,3 [20]. The interpretation would be the existence of a bottonium-like analogue to the Y(4260) called Y_b that is overlapped with the $\Upsilon(5S)$ resonance. Before solving these two problems, it is used to call the $\Upsilon(5S)$, $\Upsilon(10860)$.

The idea of this practical work will be to see if the decay $\Upsilon(5S) \rightarrow \Upsilon(4S)\pi^+\pi^-$ exist and if yes, then try to measure its branching fraction. Then, a possible anomalous in the measurement could confirm the trend of the $\Upsilon(5S) \rightarrow \Upsilon(nS)\pi^+\pi^-$ decay for n=1,2,3 and will contribute to a better accuracy of the fraction f_s (fraction of B_s compared to all B mesons).

For the $\Upsilon(4S)$, its mass is just above the $B-\bar{B}$ threshold, then it decays in a $B-\bar{B}$ pair, which is strong interaction. So the dimuon decay, which is electromagnetic decay, is suppressed. The best way would be to make an exclusive reconstruction of $\Upsilon(5S) \rightarrow \Upsilon(4S)\pi^+\pi^-$. But for B mesons reconstruction, a big sample is needed, which is not the case at $\Upsilon(5S)$ resonance. The only way with Belle sample at $\Upsilon(5S)$ is to make a partial reconstruction of $\Upsilon(4S)$ using the two pions.

A.2 Summary of Master's TPIV Results

The kinetic energy left by the $\Upsilon(5S) \to \Upsilon(4S)\pi^+\pi^-$ decay is very small, the maximum momentum available for a pion is $|\vec{p}_{max}| = 42^{+21}_{-42}$ MeV/c, where the errors come from $\Upsilon(4S)$ and pion mass error. But the $\Upsilon(4S)$ is a resonance, hence has a proper width of 20.5 ± 2.5 MeV which gives a maximum momentum for pion of ??? with 1σ less $\Upsilon(4S)$ mean mass. Due to too low pions momentum, the reconstruction efficiency is small (see Figure A.2.1), the detector can only reconstruct the most energetic pion tracks with more than 40 MeV/c momentum.

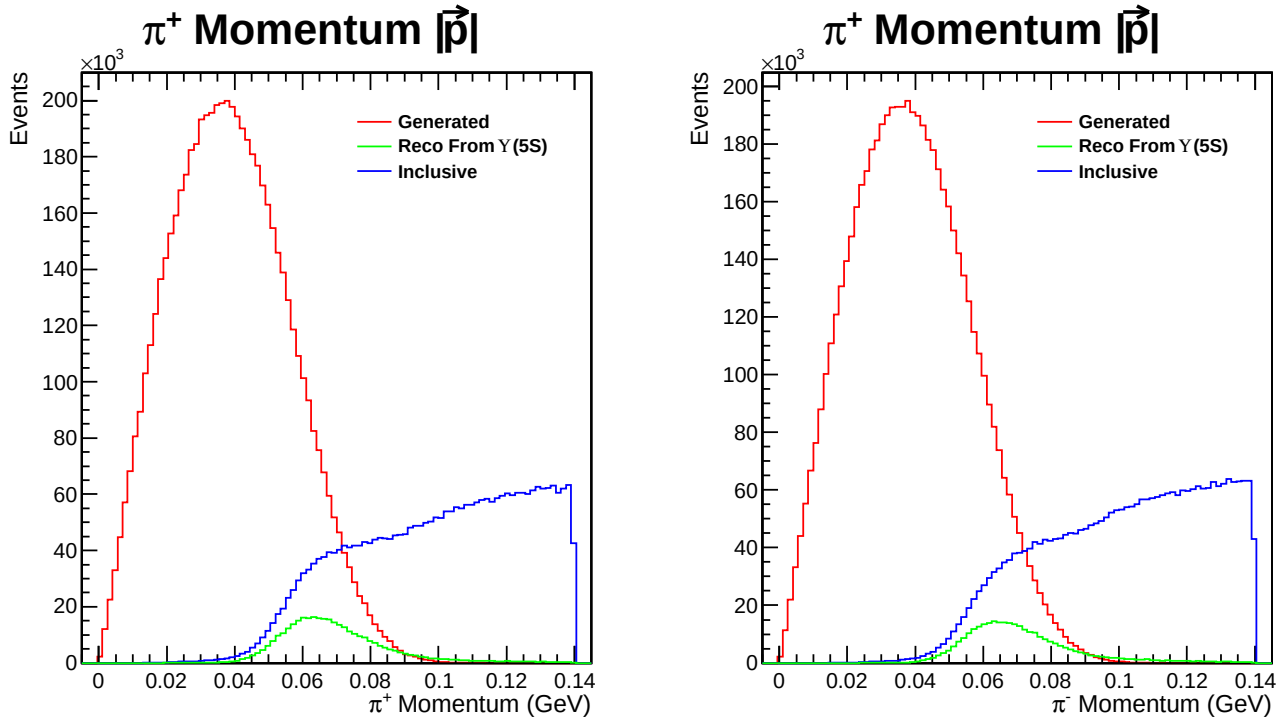

FIGURE A.2.1: π^+ and π^- momentum spectrum for generated, reconstructed $\Upsilon(5S) \to \Upsilon(4S)\pi^+\pi^-$ and inclusive pions

Combining the two pions, the Figure A.2.2 shows the events that has been reconstructed. Knowing the beam energy and combining 4-momentum of the two pions, the recoil mass can be computed. The Figure A.2.3 shows the recoil mass in $\Upsilon(4S)$ mass region using a signal MC (1 million $\Upsilon(5S) \to \Upsilon(4S)\pi^+\pi^-$ events with $\Upsilon(4S)$ decaying according to branching fractions table), where only the left part of the resonance is reconstructed. The fit is performed using events from the left to the distribution maximum with mean energy given by the PDG table.

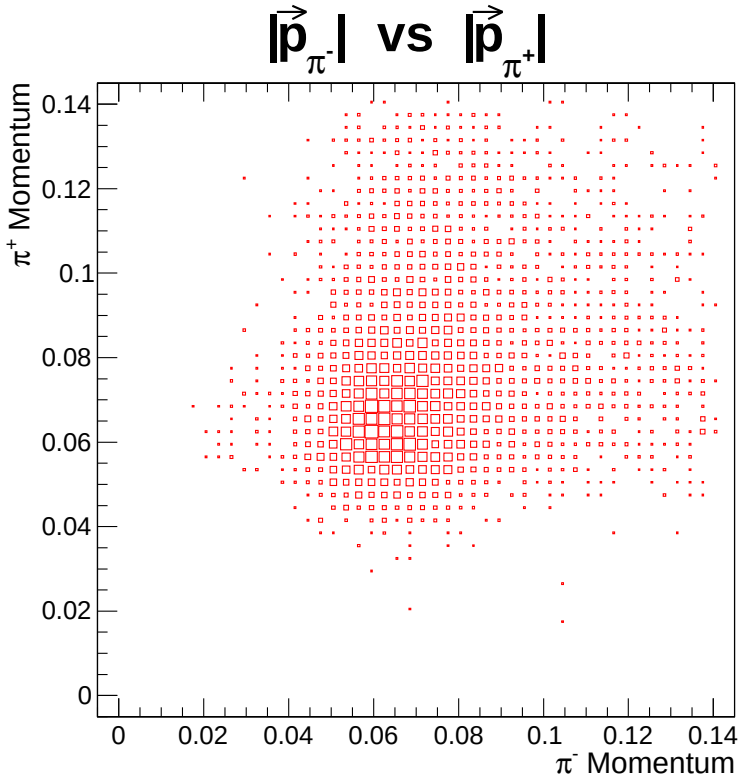

FIGURE A.2.2: $\pi^+\pi^-$ phase space of $\Upsilon(5S) \rightarrow \Upsilon(4S)\pi^+\pi^-$ decay

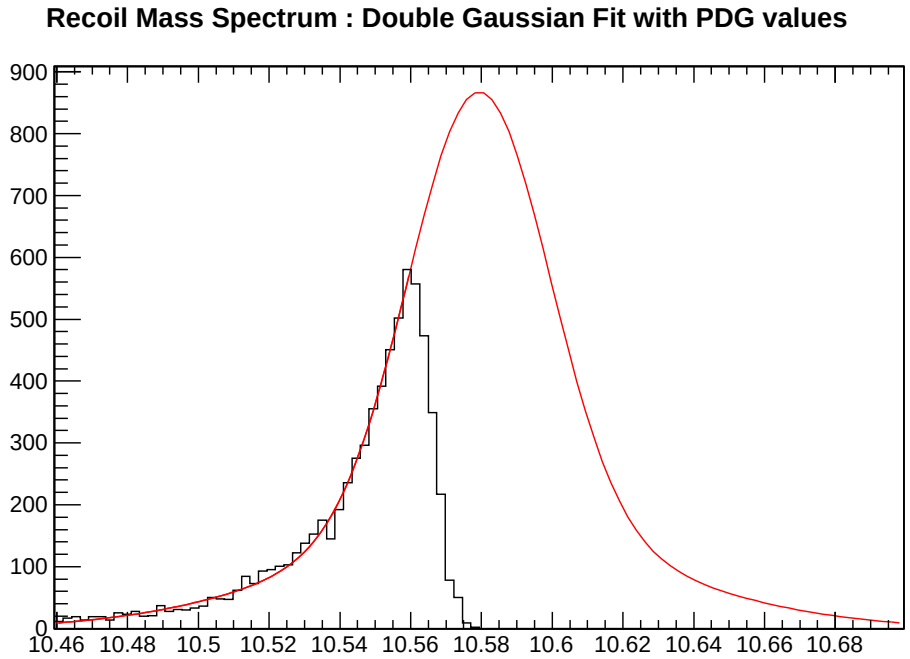

FIGURE A.2.3: Signal recoil mass spectrum with double gaussian fit with PDG values

A.3 Expected $\Upsilon(5S) \rightarrow \Upsilon(4S)\ \pi^+\ \pi^-$ yield and Recoil Mass Data Spectrum

The number of expected $\Upsilon(5S) \rightarrow \Upsilon(4S)\ \pi^+\ \pi^-$ events can be calculated with available data :

$$N_{exp}^{\Upsilon(5S)\rightarrow\Upsilon(4S)\pi^+\pi^-} = \mathcal{L}^{\Upsilon(5S)} \cdot \sigma_{e^+e^-}^{\Upsilon(5S)} \cdot \mathcal{B}(\Upsilon(5S) \rightarrow \Upsilon(4S)\pi^+\pi^-) \cdot \epsilon^{\Upsilon(5S)} = (527 \pm 26) \text{ events} \qquad \text{(A.1)}$$

with an $\Upsilon(5S)$ data integrated luminosity of $\mathcal{L}^{\Upsilon(5S)} = (23.6 \pm 0.3)$ fb^{-1}, an $\Upsilon(5S)$ production cross section of $\sigma_{e^+e^-}^{\Upsilon(5S)} = (0.302 \pm 0.014)$ nb, an expected $\Upsilon(5S) \rightarrow \Upsilon(4S)\pi^+\pi^-$ branching fraction of $\mathcal{B}(\Upsilon(5S) \rightarrow \Upsilon(4S)\pi^+\pi^-) = 1\%$ and a MC reconstruction efficiency of $\epsilon^{\Upsilon(5S)} = (0.740 \pm 0.009)$ %.

A.4 Background Suppression

Even with less than half of the recoil mass spectrum, a parametrization and a fit of the mass could be possible. To clam the discovery, a 5σ significance is required, therefore the background must be such that $B/S \lesssim 20$ with expected signal yield from previous section. Looking at the Figure A.4.1, an idea of the combinatorial background level (with events coming from $\Upsilon(4S)$ decay) can be obtained and it looks too high compared to signal yield, hence background suppression is required.

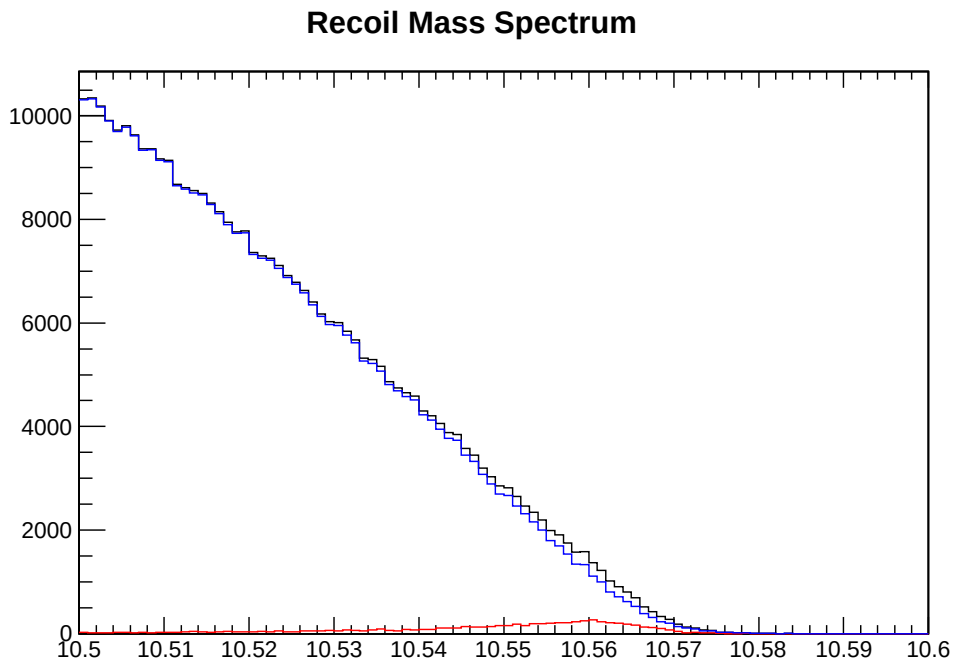

FIGURE A.4.1: Recoil mass spectrum with the signal and combinatorial background from $\Upsilon(4S)$ decay

In the TPIV project, it has been shown that kinematic cuts (pions momentum, angle between two pions in $\Upsilon(5S)$ frame) cannot be used, because these cuts destroys the recoil mass spectrum, hence only soft kinematic cuts can be applied. There is still geometric cuts that can be looked for. Four different cuts is selected : the radial distance dR of π track starting point from IP, the Z distance dZ of π track starting point from IP, the vertex fit $\chi^2_{\text{vertex fit}}$ and the Z distance ΔZ separating the $\pi\pi$ vertex from a common vertex of other tracks coming from $\Upsilon(4S)$. Figure A.4.2 shows the signal and combinatorial background spectrum of dR, dZ, $\chi^2_{\text{vertex fit}}$ and Δz from $\Upsilon(4S)$ decay.

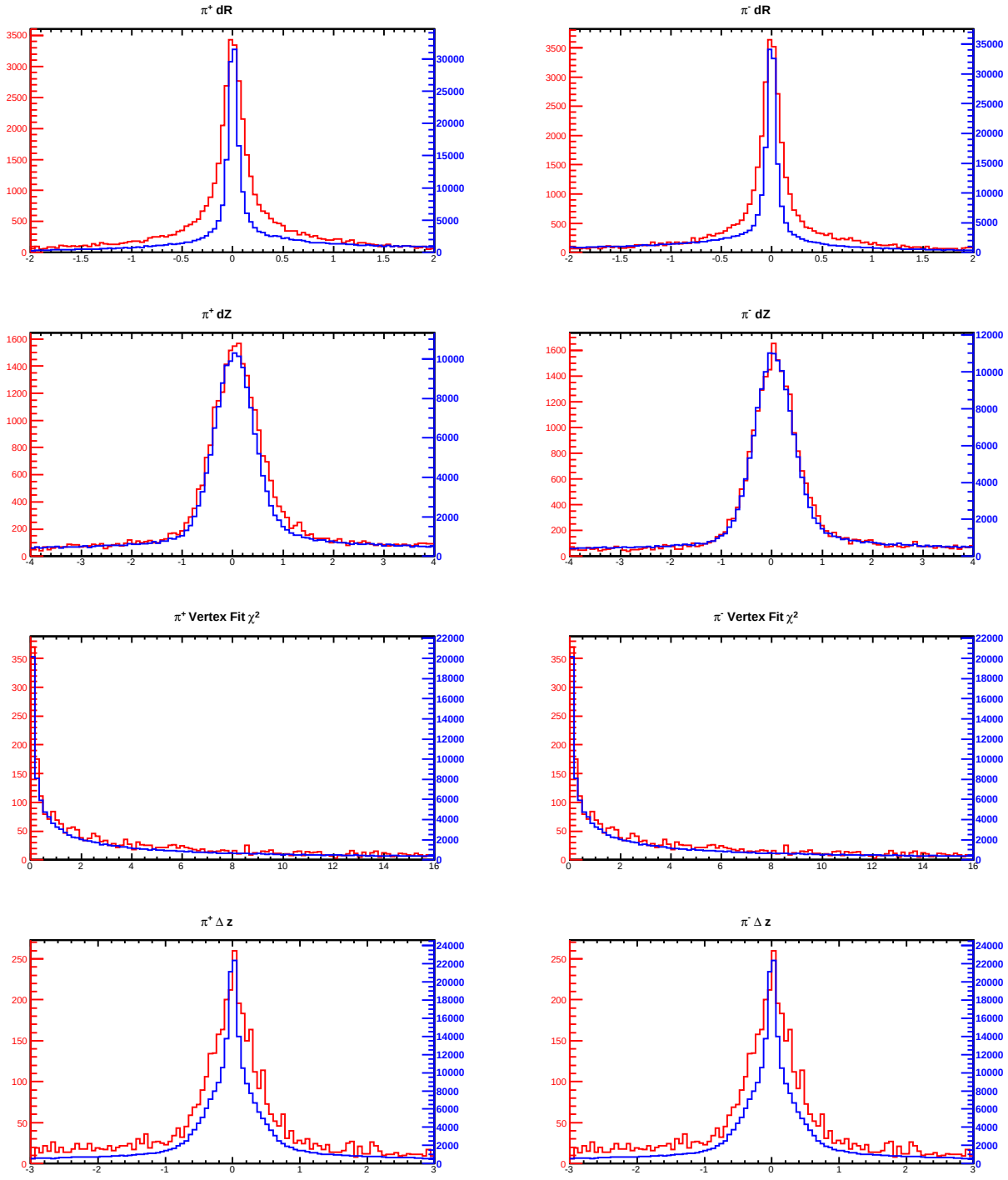

FIGURE A.4.2: dR, dZ, vertex fit $\chi^2_{\text{vertex fit}}$ and Δz for π^+ and π^- for signal and background

Looking at the results from the vertex fit $\chi^2_{\text{vertex fit}}$, signal and background spectrum are more or less the same, hence only a soft cut can be applied. The dR and dZ spectrum show bad results for this analysis, their spreads are high. But due to their low momentum, π curvature radius can be very small, hence number of hits in CDC and the low proximity of hits can lead to unprecise tracking fit. In addition, multiple scattering becomes more and more important high momentum decreasing, which leads to large fluctuations around the nominal track trajectory. Therefore, with low accuracy tracks, the dR and dZ resolution becomes high

and nothing can be done against it and only soft cuts can be applied. Then, standard looser cuts are used : $dR = 2$ cm, $dZ = 4$ cm and $\chi^2_{\text{vertexfit}} = 16$.

The idea behind the Δz cut comes from the $\pi\pi$ and the common vertex of tracks coming from $B\bar{B}$ decays which separation is given by the B lifetime, where the $\Upsilon(4S)$ decay quickly. Therefore, a non trivial Δz is expected for signal events and trivial one for combinatorial background.

Looking to the Δz in Figure A.4.2, the bad resolution smears the expected B lifetime, hence no cuts on Δz can be applied.

The last cut is the continuum suppression using R_2 which is the ratio of the second to zeroth Fox-Wolfram moment and the Figure A.4.3 shows the results for signal and background.

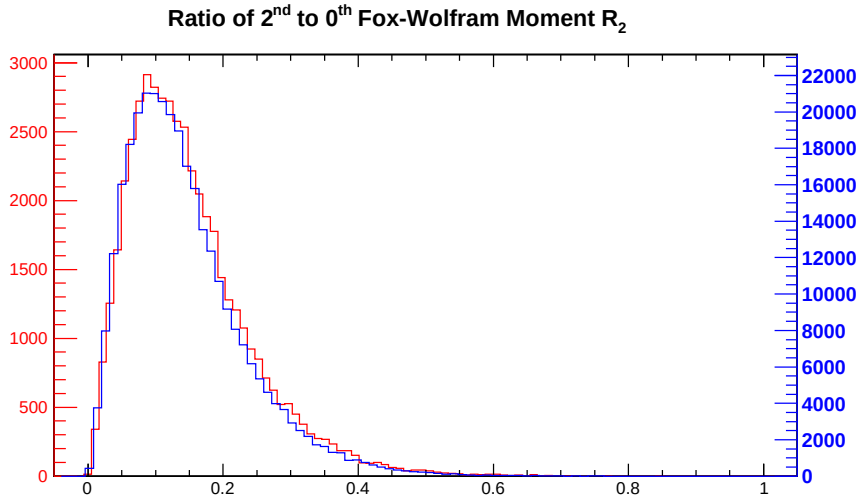

FIGURE A.4.3: R_2 for signal and background

The signal and background are the same, hence no strong cut can be applied on R_2.

No strong cut has been found to suppress combinatorial background, the background stays too high, therefore we can conclude of the invisibility of $\Upsilon(5S) \rightarrow \Upsilon(4S)\ \pi^+\ \pi^-$ decay with partial reconstruction technique at Belle.

Appendix B

Preliminary results of charged track momentum calibration using D_s mass peak position

Figure B.0.4 shows the gaussian mean μ results.

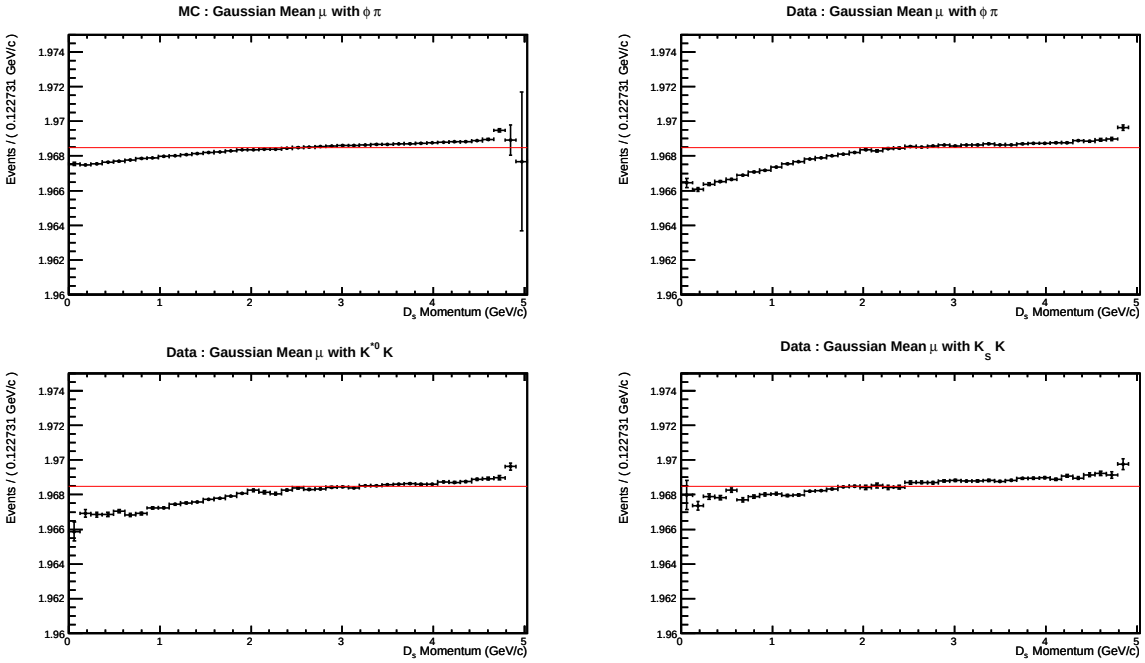

FIGURE B.0.4: Gaussian mean μ for $\phi\pi$ (MC and data), $K^{*0}K$ (data) decay and K_SK (data) decay with in red the D_s mass PDG value [9]

These plots show a momentum dependence of the gaussian mean μ. The dependence can come from the addition of two different contributions :

1. *Tracking Scale Factor* : The momentum of a given track is obtained from the helix parametrization which is strongly dependent on the magnetic field map and dE/dx knowledge (see 2.4). If these two parameters are not well known possible shift to the real D_s mass value can exist. Therefore a momentum dependence of the D_s mass peak can occur, because combination of charged tracks, due to the scale factor made of the combination of magnetic field and dE/dx values.

2. *Symmetric Double Gaussian Fitting* : The D_s mass spectrum presents a small asymmetry in the shape 5. This asymmetry can be momentum dependent, hence with a symmetric double gaussian where the two gaussian mean are the same, the mean can fluctuate to take into account the tail part. Therefore, a momentum dependence of the mean μ can rise.

A deep analysis of this momentum dependence would help to improve the tracking scale factor and the D_s mass resolution, if it turns out that this dependence is not only due to fitting.

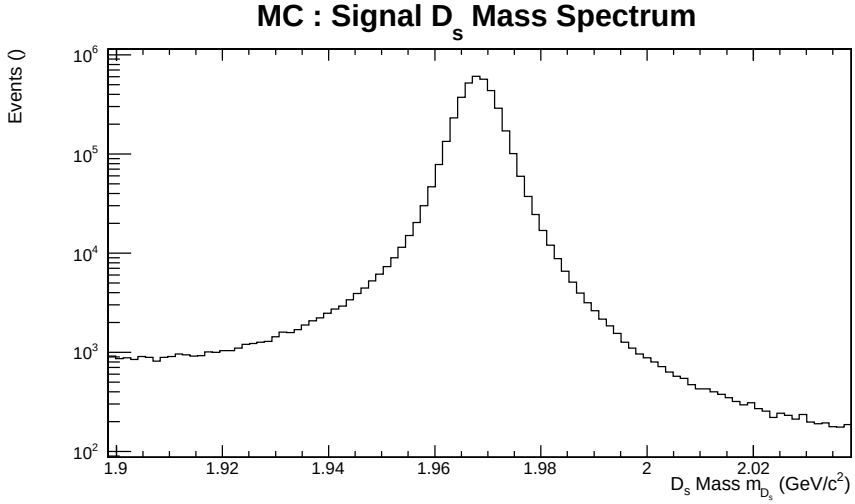

FIGURE B.0.5: Signal D_s mass spectrum with $D_s \to \phi\pi$

Acknowledgments

Many thanks to Tagir Aushev for his help on Belle physics, Belle framework and for the corrections of this report. Thanks to Rémi Louvot for his help and his answer to my questions. An finally, many thanks to Olivier Schneider for his corrections of this report and for physics discussions.

Bibliography

[1] A. Carter and A. I. Sanda, Phys. Rev. Lett. **45**, 952 (1980); M. Bander, D. Silverman, and A. Soni, Phys. Rev. Lett. *43*, 242 (1979).

[2] B. Aubert *et al.* (*BABAR* Collaboration), Phys. Rev. Lett. **94**, 161803 (2005); K. Abe *et al.* (Belle Collaboration), Phys. Rev. D **71**, 072003 (2005); **71**, 079903(E) (2005); B. Aubert *et al.* (*BABAR* Collaboration), Phys. Rev. Lett. **98**, 031801 (2007); K.-F. Chen *et al.* (Belle Collaboration), Phys. Rev. Lett. **98**, 031802 (2007).

[3] B. Aubert et al. (*BABAR* Collaboration), Phys. Rev. Lett. **93**, 131801 (2004).

[4] Y. Chao et al. (Belle Collaboration), Phys. Rev. Lett. **93**, 191802 (2004).

[5] J. Charles et al. (CKMfitter Group), Eur. Phys. J. C **41**, 1 (2005); M. Bona *et al.* (UTfit Collaboration), J. High Energy Phys. **07** (2005) 028.

[6] N. Cabibbo, Phys. Rev. Lett. **10**, 531 (1963); M. Kobayashi and T. Maskawa, Prog. Theor. Phys. **49**, 652 (1973).

[7] M. Bona et al. (UTfit Collaboration), Phys. Rev. Lett. **97**, 151803 (2006).

[8] A. Carter and A. I. Sanda, Phys. Rev. Lett. **45**, 952 (1980); Phys. Rev. D **25**, 85 (1981); I.I. Bigi, A.I. Sanda, Nucl. Phys. B **193**, 85 (1981).

[9] C. Amsler *et al.* (Particle Data Group), Phys. Lett. **B667**, 1 (2008).

[10] A.K Giri *et al.*, Eur. Phys. J. C **22**, 115-121 (2001).

[11] A. Zupanc *et al.* (Belle Collaboration), Phys. Rev. D **75**, 091102(R) (2007).

[12] B. Aubert et al. (*BABAR* Collaboration), Phys. Rev. D 65, 091104(R) (2002).

[13] V. Jain, Nucl. Phys. B Proc. Suppl. **50**, 96 (1996); CLEO Collaboration, T. E. Coan *et al.*, Phys. Rev. Lett. **80**, 1150 (1998).

[14] I. Bigi et *al.*, Phys. Lett. B **323**, 408 (1994).

[15] A. F. Falk, M. B. Wise and I. Dunietz, Phys. Rev. D **51**, 1183 (1995).

[16] F. Fang, Belle Note #323, unpublished (2000).

[17] D. Besson *et al.*, Phys. Rev. Lett. **54**, 381 - 384 (1985).

[18] D.M.J. Lovelock *et al.*, Phys. Rev. Lett. **54**, 377 - 380 (1985).

[19] K.-F. Chen *et al.* (Belle Collaboration), Phys. Rev. Lett. **100**, 112001 (2008).

[20] I. Adachi *et al.* (Belle Collaboration), arXiv:0808.2445 [hep-ex].